High-pressure phase transition and phase diagram of gallium arsenide

J. M. Besson, J. P. Itié, A. Polian, and G. Weill
Physique des Milieux Condensés, Université Pierre et Marie Curie, T13-E4, 4 place Jussieu, F-75252 Paris CEDEX 05, France

J. L. Mansot
Laboratoire de Physique Cristalline, Institut des Matériaux de Nantes, 2 rue de la Houssinière, F-44072 Nantes, France

J. Gonzalez
Centro de Estudios de Semiconductores, Facultad de Ciencias, Universidad de los Andes, La Hechicera, Merida 5201, Venezuela

(Received 3 August 1990; revised manuscript received 25 April 1991)

Under hydrostatic pressure, cubic GaAs-I undergoes phase transitions to at least two orthorhombic structures. The initial phase transition to GaAs-II has been investigated by optical-transmittance measurements, Raman scattering, and x-ray absorption. The structure of pressurized samples, which are retrieved at ambient, has been studied by x-ray diffraction and high-resolution diffraction microscopy. Various criteria that define the domain of stability of GaAs-I are examined, such as the occurrence of crystalline defects, the local variation in atomic coordination number, or the actual change in crystal structure. These are shown not to occur at the same pressure at 300 K, the latter being observable only several GPa above the actual thermodynamic instability pressure of GaAs-I. Comparison of the evolution of these parameters on increasing and decreasing pressure locates the thermodynamic transition region GaAs-I→GaAs-II at 12±1.5 GPa and at 300 K that is lower than generally reported. The use of thermodynamic relations around the triple point, and of regularities in the properties of isoelectronic and isostructural III-V compounds, yields a phase diagram for GaAs which is consistent with this value.

I. INTRODUCTION

Solid-solid phase transitions have been one of the first subjects of study in the early days of high-pressure research. Indeed, the knowledge of thermodynamic phase boundaries and the measurement of density versus pressure and temperature are complementary in order to establish the equation of state (EOS) of a given system, which is a necessary, but far from sufficient condition to define the form of interatomic potentials at short distance. The understanding of interatomic (intermolecular) potentials is now in rapid progress with the advent of experimental methods which directly measure interatomic distance under pressure, such as single-crystal x-ray diffraction, x-ray-absorption spectroscopy, (XAS), and elastic neutron scattering. This is complemented by those measurements which give access to interatomic interactions (restoring forces) such as Raman scattering and infrared absorption for the high-frequency motion of atoms and Brillouin scattering which involves low-frequency (quasi)static deformations and will, ideally, provide the full tensor of elastic constants of a given solid under pressure.

Theoretical calculations also have made significant progress in the last decades and early methods, based on empirical scaling rules, have been replaced by total-energy calculations based on pseudopotentials with a minimum of empirical input. A crucial test of these methods is the prediction of solid-solid phase-transition pressures. A calculation will only predict the thermodynamic equilibrium pressure, if it exists, or the pressure-temperature domain where two given structures will have the same free energy. As we shall see further on, this may be completely different from the pressure where the phase transition is observable. Even if we forget the uncertainty coming from pressure inhomogeneity, errors on the pressure scale and such experimental imperfections, the main problem in locating a solid-solid phase transition lies in that the various physical parameters which characterize a solid in the low-pressure phase do not simultaneously change in a discontinuous manner at a first-order phase transition. This is only an ideal case. Several physical parameters are examined in the present paper: Optical transmittance, atomic coordination and interatomic distances, and the space group of the lattice. These parameters do indeed vary as expected at the phase transition but not at the same pressure, at 300 K.

The only systematic investigation of the phase diagram of the III-V semiconductors at variable temperature and pressure was the pioneer work of Jayaraman and coworkers.[1–3] These results were largely the basis for theoretical evaluations notably by Phillips,[4] and then Van Vechten[5–7] using quantum dielectric theory and scaling procedures for the electronegativity difference among constituent atoms. In the past two decades a large amount of work, both experimental, mainly at room temperature, and theoretical, using the pseudopotential methods has been devoted to the group-IV-element and

III-V-compound series, notably GaAs, as regards its structural and vibrational properties under pressure.

The phase transition GaAs-I→GaAs-II had previously been located[8,9] around 17 GPa, before being lowered to 16.6 GPa or less,[10] and an orthorhombic structure for GaAs-II with space group $Pmm2$ was proposed. GaAs-III with space group $Imm2$ occurs above 24 GPa, as well as simple hexagonal GaAs-IV, above some 60 GPa.[10] Their EOS has been reported in the same paper and fits previously published data.[11]

Other properties of GaAs such as Raman scattering under high pressure[12] and the variation of its energy gap and optical absorption edges[11,13–15] have been investigated and give a reasonably coherent picture of this semiconductor up to the transition pressure. One study of GaAs with dynamic (shock-wave) methods reports[16] the only observation of the phase transition at temperatures higher than 300 K for complete transformation of GaAs-I to GaAs-II that is 16.3 GPa at 360 K $< T <$ 370 K.

The theoretical situation has been somewhat uncertain regarding predictions on GaAs-II. Before its orthorhombic structure was reported, only one paper[17] had predicted it as a consequence of the orthorhombic symmetry of the displacements of atoms due to a TA(X) phonon. Other calculations of the stability of high-pressure structures[18,19] only considered the β-Sn, NaCl, or NiAs lattice as probable candidates. The predictions on the phase-transition pressure are rather dispersed: 8 GPa in Ref. 17, 15.3 GPa in Ref. 7, 16.7 GPa in Ref. 19, and 17 GPa in Ref. 18.

In this paper, the phase transition in GaAs has been investigated *in situ* by measurements of the optical transmittance, x-ray absorption, and Raman scattering. The structure of recovered samples which had been pressurized to different pressures in the transition region has been studied, in addition, by x-ray diffraction and high-resolution electron microscopy. Thus the following points will be examined.

(i) In the next section, the optical properties of GaAs at 300 K below, at, and above, the phase transition up to 17 GPa only, in order to be below the full I→II transformation pressure, both on the upstroke and downstroke.

(ii) In Sec. III we analyze the structure of pressurized samples which have been retrieved at ambient, from single crystals as a starting material. This is in contrast with previous x-ray work where powder samples were used. The Debye-Scherrer diagram of oriented single crystals is quite sensitive to misorientations of microcrystals when defects appear and thus allows one to detect the first structural defects due to the transition. The structure of those defects is evidenced by high-resolution electron microscopy. The optical-absorption edge at ambient shows partial amorphization on the reverse II→I transition.

(iii) Coordination changes around Ga atoms are studied by x-ray absorption under pressure and discussed in Sec. IV. Full transition to GaAs-II and GaAs-III was achieved in those experiments in order to investigate the extreme limits of stability for fourfold and sixfold coordination, on the upstroke and downstroke.

(iv) In Sec. V, Raman scattering on the LO and TO phonons proves to be a sensitive gauge for locating the reverse II→I transformation. Putting together those data and comparing them with previous results on x-ray diffraction under pressure lead us, in Sec. VI, to propose, for the thermodynamic transition pressure of GaAs, 12±1.5 GPa at 300 K, which is lower than the generally accepted value. This large discrepancy between 12 GPa and the actual observation (> 16 GPa) of the transformation can be accounted for by the nature of the instability in the (111) planes of the structure. It is shown, moreover, in Sec. VII, that this value can be derived, using thermodynamic arguments and comparisons with other compounds, solely from previously published portions of the GaAs phase-boundary lines, and allows one to construct a coherent phase diagram for this solid.

II. OPTICAL MEASUREMENTS UNDER PRESSURE

The aim of the measurements described in this section was to locate the pressure for the cubic to orthorhombic transition at 300 K by observing and analyzing the irreversible increase of the optical absorption of the crystal at the phase transition. To evaluate the irreversible absorption that sets in under pressure, the intrinsic absorption of zinc-blende-structure GaAs has to be known even above the phase-transition point where it is no longer measurable. For this, an extensive set of measurements was done up to 12 GPa and the full shape of the absorption edge could be interpreted in terms of the band parameters under pressure.[14] It is then possible to extrapolate the variation of the zinc-blende-structure GaAs band-edge absorption in the small pressure range where it is necessary to subtract it. This work will not be fully described here and will be reported in a forthcoming paper.

A. Experiment

GaAs samples were grown by molecular-beam epitaxy at the Standard Telecommunications Laboratory (United Kingdom). The orientation of the layers was (100) with $n \sim 10^{15}$ electrons/cm^3. Mechanical polishing was used to remove the substrate and thin the samples down to thicknesses between 20 and 30 μm. After etching, these were cleaved to square slabs some 100 μm on the side. A classical lever-arm diamond-anvil cell (DAC) was used. Anvils were 0.3-carat stones with 0.6-mm culets. The sample hole in the Inconel gasket was typically 300 μm in diameter and 80 μm in thickness, to start with. The pressure was calibrated using the power-five ruby luminescence scale with the pressure in GPa related to the wavelength λ by

$$P = 380.8[(\lambda/\lambda_0)^5 - 1] . \quad (1)$$

The 514.5- and 488-nm lines of an argon laser were used at powers of a few milliwatts. Ruby samples were $\sim$4000 ppm Cr^{3+} doped and 5 to 15 μm in average dimensions. For transmission measurements, white light was focused through a Diaver metallographic microscope to a spot smaller than 50 μm. To reduce stray light, a precollimation diaphragm was inserted between the source and the sample at a focal point of the system and a second iris was located in the ocular focal plane of the

microscope. The beam was then focused onto the entrance slit of a T 800 Coderg triple monochromator which covers a spectral range from 1.4 to 2.5 eV. Experimentally, stray-light levels with this setup were in the range of $(2-3)\times10^{-4}$, allowing measurements of the absorption coefficient $\alpha\sim(4-2)\times10^{3}$ cm^{-1} for samples 20 to 30 μm in thickness. Several pressure media were used: argon, the 4:1 ethanol-methanol mixture, or silicone oil, in the order of decreasing hydrostaticity. This was done to measure the influence of inhomogeneous stress on the occurrence of the solid-solid phase transition.

The transmittance was measured by comparing the light flux through the sample and the transparent pressure transmitter in the cell, on the side of the crystal. The refractive index had been determined separately by the interference fringes method. In all cases, a geometrical correction factor was used before calculating α, to scale the apparent transmittance to its theoretical value of $(1-R)/(1+R)$ (R is the reflectivity) in regions where αd is known to be negligible. The absorption edge at pressures up to 12 GPa was analyzed with the Elliott[20] model and its later modifications[21] for the direct edge. The indirect transition was accounted for along Dumke's formulation.[22] A multiparameter adjustment on the effective masses, rydberg of the exciton, oscillator strengths, and band edges yielded a fit with experiment which is good enough for the present purpose, that is, extrapolation from 12 to 16 GPa. Figure 1 shows examples of the fit (dashed line) with experiment (solid lines) at three different pressures. The band edges, among other parameters, were extrapolated along the polynomials given in the caption.

B. Results

Above some 13 GPa, extra absorption comes in and remains, on depressurization. The intensity of the process increases with increasing pressurization up to some 17 to 18 GPa when the crystals rapidly opacify. In this subsection we shall examine separately the upstroke and downstroke evolution of GaAs.

1. Pressurization

Several pressure media were used. We shall describe results with two of them: the ethanol-methanol mixture, and argon. Figure 2 shows the absorbency at 12.2 GPa of a 20-μm-thick sample after successive pressurization in the ethanol-methanol mixture, to the maximum pressures indicated on the figure. In this particular set of experiments, 12.2 GPa was taken as the starting pressure because repeated measurements showed that the behavior of GaAs was reversible when not taken above some 12 GPa. Each of the other four curves shows the spectrum taken at 12.2 GPa, after the sample had successively been pressurized to higher pressures, indicated in the figure, then taken back to 12.2 GPa and measured. After subtracting the absorbency due to zinc-blende-structure GaAs at 12.2 GPa, the extra absorption was expressed as an equivalent absorption coefficient α_D which could be fitted to a power law of $h\nu$, the photon energy: $\alpha_D = A(h\nu)^n$, where A is a constant and n, the exponent, is between 3 and 4 at the highest pressurization value. This residual absorption, shown on a log-log scale in Fig.

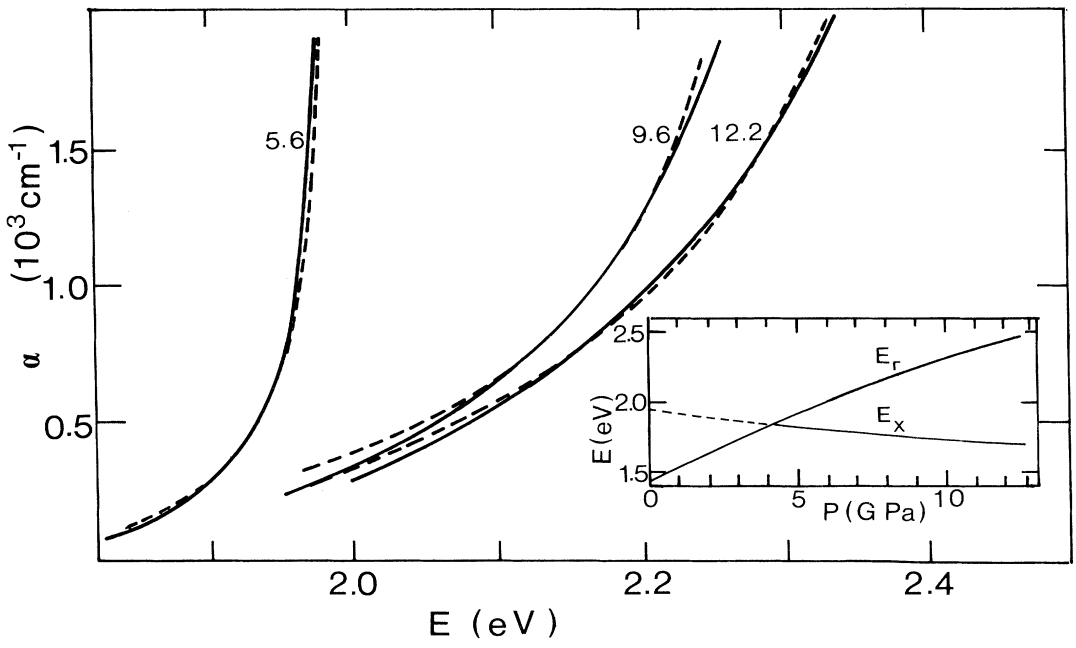

FIG. 1. Absorption coefficient vs photon energy of GaAs at 300 K for three different pressures (in GPa). Solid lines, experiment. Dashed line, fit as explained in text. Inset, variation with pressure of the direct (E_Γ) and indirect (E_X) energy gaps, obtained from the fit of the absorption edge as explained in the text. The energy of the gaps varies with pressure as E_Γ (eV)$=1.427+11.5\times10^{-2}P-24.5\times10^{-4}P^2$, and E_X (eV)$=1.950-2.6\times10^{-2}P+4.7\times10^{-4}P^2$.

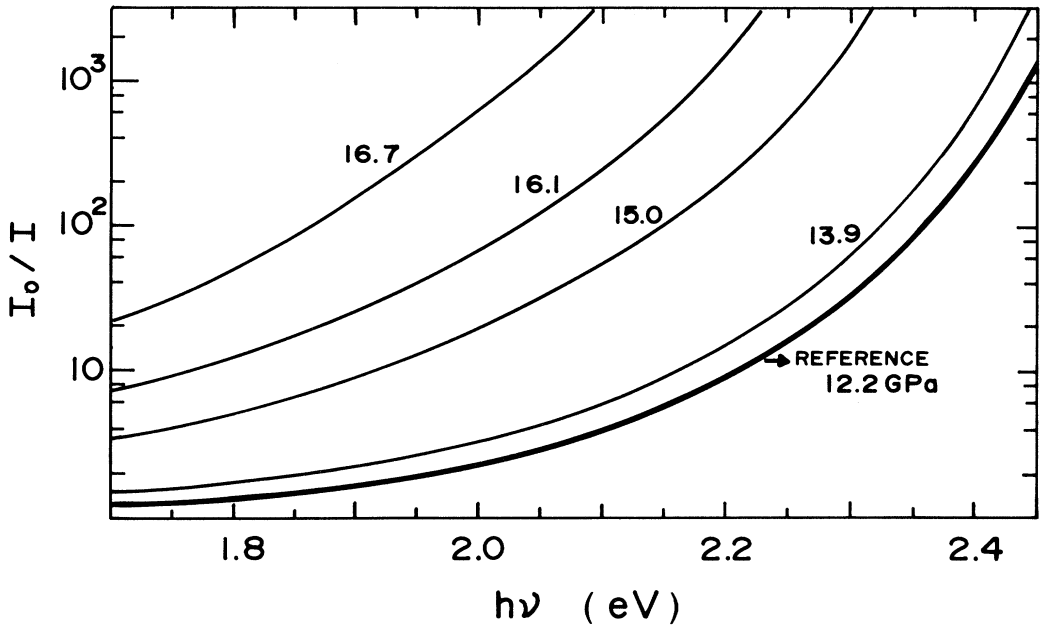

FIG. 2. Absorbency (logarithmic scale) of a 20-μm slab of GaAs at 12.2 GPa. Figures indicate the successive pressurization values (GPa) for the samples but all five spectra are measured at 12.2 GPa, on the downstroke.

3, increases approximately linearly at any photon energy with increasing pressure. Conversely, extrapolation of its intensity to lower pressures shows it to be zero at 13.6 GPa in the ethanol-methanol mixture. Results in argon are analogous, the main difference being that irreversible processes occur at a higher pressure, close to 15 GPa in this case.

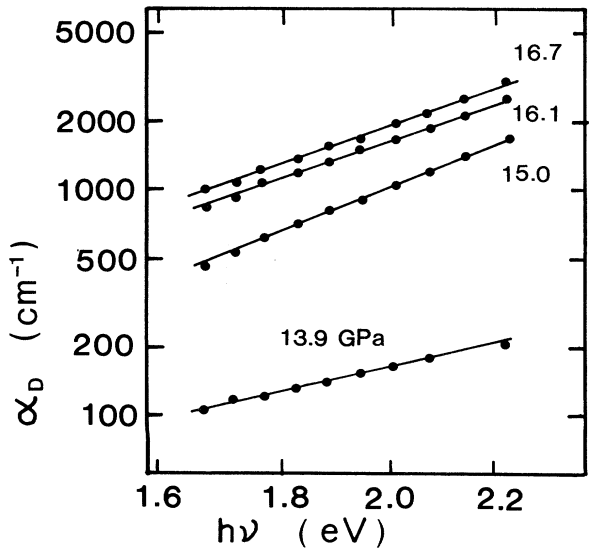

FIG. 3. Irreversible additional absorbency at 12.2 GPa of samples successively taken to the maximum pressure (GPa) indicated on the figure. This absorbency is expressed as an equivalent absorption coefficient α_D for a 20-μm-thick sample.

2. *Depressurization*

Full transformation to the orthorhombic structure occurs, as a rule, in the vicinity of 20 GPa but, even at 18 GPa, the samples are too opaque to be studied by optical methods. Thus studies on the downstroke were done on samples where the transition had just been initiated so that their transmittance remained within experimentally accessible limits. After a sample has been partly transformed by pressurization in the range of 16 to 17 GPa, its behavior can be observed all the way down to ambient and the residual absorption extracted from the total, since the absorption edge of zinc-blende-structure GaAs is known. The zinc-blende-structure GaAs absorption edge can be calculated at all pressures to 12 GPa, or above, by use of Elliott's[20] and Dumke's[22] equations for the direct and indirect edges, and of their pressure dependence, which is given by the polynomials in the caption of Fig. 1. Figure 4 shows examples of the absorption edges of a crystal that was pressurized to 16.6 GPa and taken down to ambient in successive steps. The residual absorption is represented at each pressure by the difference, on a logarithmic scale, between the dashed and solid curves. In Fig. 5, this α_D is plotted on a logarithmic scale as before. Some noteworthy features are as follows: (i) The residual absorption does not vary much down to some 10 GPa. It increases in intensity afterwards, down to ~7 GPa. (ii) The slope of the log-log lines remains the same down to ~7 GPa, about 3.8 in the present case. Afterwards, the slope itself increases rapidly down to ambient where it is close to 8.

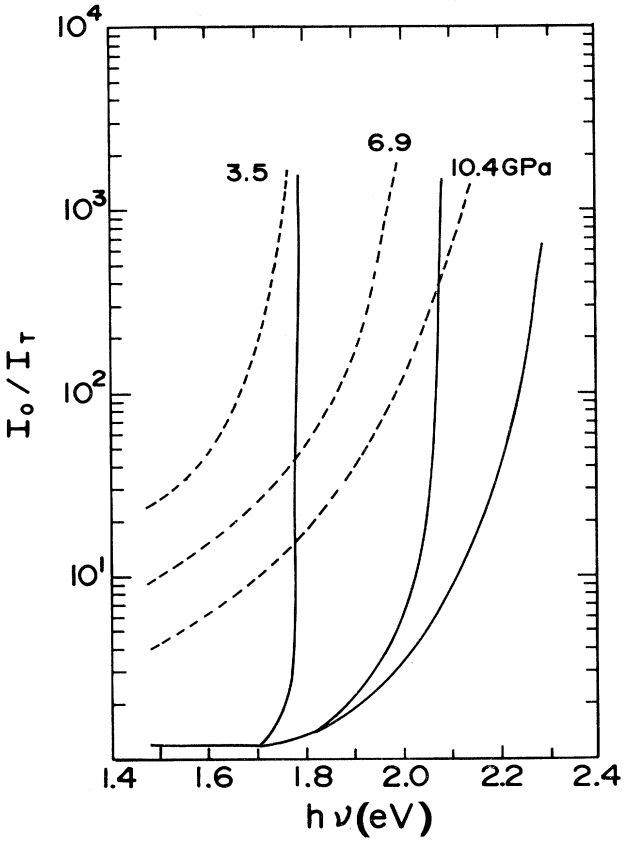

FIG. 4. Absorbency (logarithmic scale) of a 20-μm GaAs sample. Solid lines, absorbency on the upstroke. Dashed lines, absorbency of the same sample at the same pressures, on the downstroke from a maximum pressure of 16.6 GPa.

3. *Analysis and discussion*

The irreversibility of the optical behavior above 13 GPa on the upstroke can be traced to the transition to the high-pressure phase. GaAs-II is probably metallic or semimetallic, and, in any case, opaque in the visible region. Local microclusters occur in the crystal where the coordination changes from fourfold in GaAs-I to sixfold in GaAs-II and GaAs-III. There, faulted regions—phase II may not yet be organized—diffuse light and reduce the transmittance by diffusion rather than by absorption. This is reflected in the power law of the apparent absorption α_D which is typical of a Mie-Grüneisen diffusion law where the exponent n may vary from 2.5 to 4, depending on the size of particles, their optical dielectric function, and that of the matrix, among others. It is clearly distinguishable from that of a finite-band-gap semiconductor where α would be a function of $(h\nu - E_g)$, E_g being some characteristic gap energy. It is also different from a metallic free-carrier absorption with a Drude-Zener $(h\nu)^{-2}$ dependence. The existence and the fine structure of those defects will be shown in the next section by electron microscopy.

The fact that this irreversible transformation starts at lower pressure (13.6 GPa) in the ethanol-methanol mixture than in argon ($\sim$15 GPa) is simply related to the higher stress inhomogeneity in the former. This is a general observation in reconstructive phase transitions that stress gradients—shear stress—will induce the phase transformation and, conversely, that hydrostatic conditions will conserve the low-pressure phase metastably further away from the equilibrium pressure, on the upstroke. Therefore in argon, the transition pressure is vastly overshot, whereas in the ethanol-methanol mixture, shear

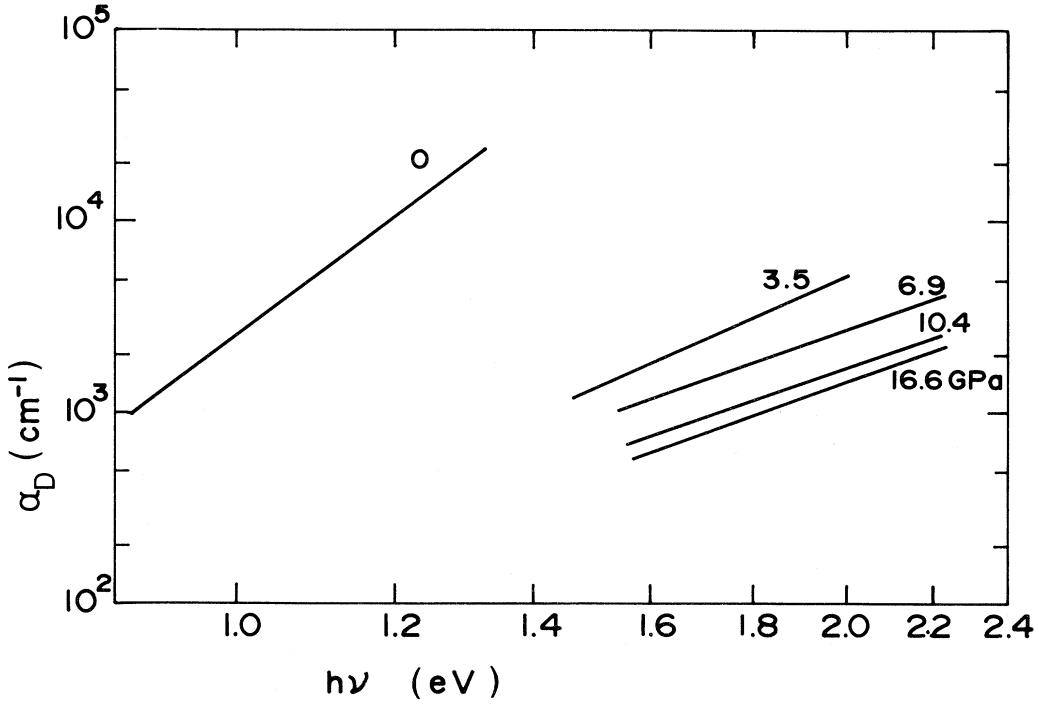

FIG. 5. Irreversible additional absorption α_D (log-log scale) of a sample taken to 16.6 GPa at successive decreasing pressures (GPa).

induces it as low as 13.6 GPa, which is nevertheless surely still above the true thermodynamic transition pressure. The increase in the intensity of α_D with increasing pressure in Fig. 3 is simply due to the increasing number of phase-II centers. On the downstroke, little happens from 16 down to about 10 GPa. The increase of α_D between 10 down to 7 GPa will be shown to be related to the backward transformation of sixfold-coordinated phase II into faulted fourfold-coordinated GaAs (Sec. V) and the increase of n from 3.8 to 8 below 7 GPa will be interpreted, in the next section, as transformation of a small fraction of the crystal to amorphous GaAs-I. The main result of this section are the following.

(i) GaAs-I is unstable above 13.6 GPa on the upstroke.

(ii) Partly transformed crystals do not show any evolution of their optical spectrum down to ~10 GPa on the downstroke.

III. STRUCTURE OF PRESSURIZED SAMPLES AT AMBIENT

In this section we shall examine results from Debye-Scherrer x-ray patterns, optical measurements in transmission, and photoconductivity, and finally high-resolution transmission electron microscopy, in all cases at ambient temperature and pressure, on pressurized samples taken out of the DAC. After undergoing the I→II→I transitions, the samples are retrieved with only slight distortions from their original shape. Since, as we shall see later on, the structure is highly disordered and microcrystalline, the microscopic structure of the sample is that of a cold isostatically pressed (CIP) compact, especially for fully transformed samples, after pressurization above 18 GPa.

A. X-ray diffraction

Single-crystalline samples were compressed in the ethanol-methanol mixture at pressures in the range of 14 to 21 GPa and taken back to ambient at a rate of about 2 GPa/min. Debye-Scherrer diagrams were then taken with the Cu $K\alpha$ line with 24-h exposure times. Before the transition, the samples exhibit the classical [100] spots of the single crystal. After pressurization to 14 GPa, weak circles appear in the retrieved samples patterns, indicating the onset of crystalline disorder after the 0 GPa→14 GPa→0 GPa cycle. Samples which have been pressurized to 17, 19, and 21 GPa give a pattern[23] which contains diffraction circles with increasing intensity, at the expense of the intensity of spots. The 21-GPa sample diagrams are perfect powder patterns. Six identifiable lines were indexed in the patterns with no appreciable differences in the interreticular distances from sample to sample, and in accord with previously published values[24] (Table I). No other ordered phase could be identified. Any other structural modification present would have to be disordered or amorphous. Indeed in the latter case, the weak diffraction halo of a-GaAs would not show even if 10% of the sample were amorphous, with the present method.

TABLE I. Comparison of observed diffraction lines in retrieved GaAs samples with those in untransformed cubic GaAs from Ref. 24.

h	k	l	d (Å) Present work	d (Å) Ref. 24
1	1	1	3.258	3.263
2	2	0	1.996	1.9982
3	1	1	1.699	1.7046
4	0	0	1.411	1.4136
3	3	1	1.294	1.2972
4	2	2	1.153	1.154

B. Optical transmittance

It was indicated that the transmission at ambient of samples pressurized to 16.6 GPa could be represented by a power-8 law. This obviously cannot be a diffusion law: no known process can account for this behavior. Now, a power-3 to -4 dependence on α_D, although it does not prove that the process is diffusion, can nevertheless be assigned to it, which we did. An apparent power-8 dependence cannot be assigned to diffusion, which means that it is not. Figure 6 shows another representation of α_D at

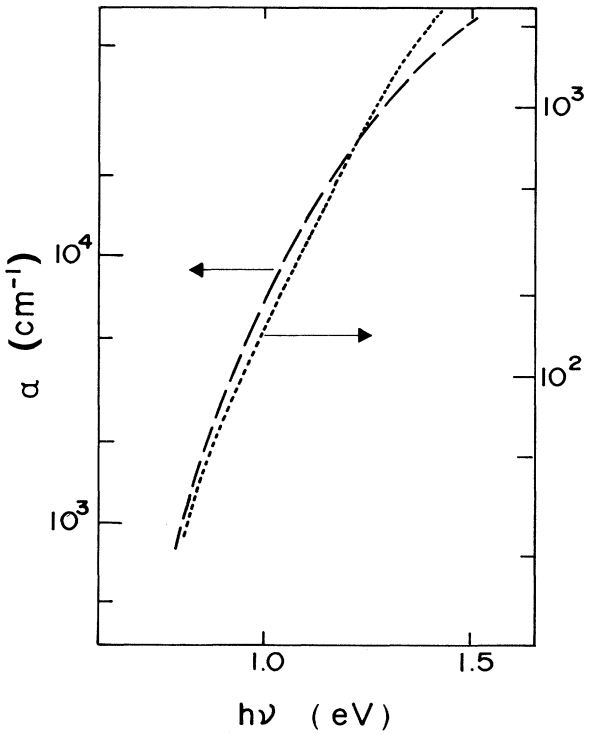

FIG. 6. Apparent absorption coefficient (logarithmic scale) of a pressurized sample of GaAs at ambient. Dotted line, right-hand scale: The absorption coefficient was calculated from the transmittance of a 20-μm-thick sample. Dashed line, left-hand scale: Measured absorption coefficient of an amorphous GaAs layer (Ref. 25). The right- and left-hand ordinate scales have been arbitrarily shifted vertically in order to superpose the two spectra.

ambient for a sample pressurized to 17 GPa (dotted line), compared with the absorption coefficient[25] of *a*-GaAs (dashed line). The similarity between the two is obvious within a scaling factor of 40 (the left- and right-hand scales were shifted vertically to superpose the two curves). The optical behavior of these samples coincides with that of an *a*-GaAs sample 40 times thinner than the actual crystal, or with that of a crystal the same size, with 2.5% *a*-GaAs. The diffusion part no longer gives any appreciable contribution, as expected for *c*-GaAs mixed with *a*-GaAs, which is also a semiconductor with a similar refractive index.

C. High-resolution electron microscopy

1. Experiment

The study was carried out on a Philips EM 120 twin transmission instrument with the following characteristics: accelerating voltage, 120 kV; condenser aperture, 150 μm; objective aperture, 70 μm; and filament, LaB_6. Point-to-point resolution was 0.34 nm and lattice resolution, 0.2 nm. Pressurized samples (~ 100 μm in diameter and 20 to 30 μm in thickness) were crushed in isopropanol. After ultrasonic dispersion, a drop of the mixture was deposited on a carbon grid. After the isopropanol has evaporated, the samples were introduced into the microscope.[26,27]

2. Results

Completely transformed samples which have been taken to a maximum pressure $P_{max} > 25$ GPa are wholly disordered material with microcrystals in the range of 5 to 10 nm, when identifiable. This high degree of disorder is expected since, under those conditions, the samples have undergone two phase transitions[10] to GaAs-II, and then to GaAs-III with a volume change close to 20%. When P_{max} is between 15 and 18 GPa, recovered samples exhibit characteristic planar defects. Figure 7(a) shows twinning planes in a sample pressurized to 17 GPa. The diffraction pattern on a 3-μ-diam area [Fig. 7(b)] confirms that the recovered sample is wholly zinc-blende-structure GaAs-I. The $(\bar{1}\,\bar{1}1)$ twinning planes separate untransformed regions from regions which have undergone transition to GaAs-II and back, leaving behind a rotation (close to 60°) of the atomic pattern with respect to the initial arrangement. This is directly observable in Fig. 7(c), which is a lattice fringe image showing, at higher magnification, the misorientation of the transformed and untransformed regions. The twinning planes are all perpendicular to the $[\bar{1}\,\bar{1}1]$ direction. These defects which extend over tens of lattice parameters normal to the plane of the figure, in the $(\bar{1}\,\bar{1}1)$ plane, are typical of a martensitic-type transition which is characterized by an instability propagating along well-defined crystalline directions. This observation alone would not be sufficient to prove that the transformed regions were indeed a backward transformation from orthorhombic GaAs on the downstroke but *in situ* x-ray diffraction[10] and x-ray absorption (Sec. IV) leave no doubt that, at that pressure, a fraction of the crystal had indeed transformed to GaAs-II with sixfold coordination around the atoms.

D. Analysis and conclusions

The different pieces of evidence obtained from this section can now be fitted together: crystalline disorder sets in between 14 and 17 GPa. The I→II transition proceeds along unstable (111) planes and these defects are responsible for the diffusive behavior that sets in. It should be noted here that the diffusion itself might originate from larger (500–2000 Å?) regions of the crystal with a high concentration of twinning since the size of the defects in Fig. 7(c) is much too small to individually diffuse light. The results of the reverse transformation back to the original zinc-blende structure is to leave a few percent of the atoms, along the twinned regions, in a locally disordered environment. Electronic levels on those sites apparently are perturbed in a similar way as in *a*-GaAs, although the geometry is quite different. In any case, they do yield an absorption behavior (Fig. 6) which is very similar to that of *bona fide* amorphous GaAs. The structure of those transformed regions now gives a

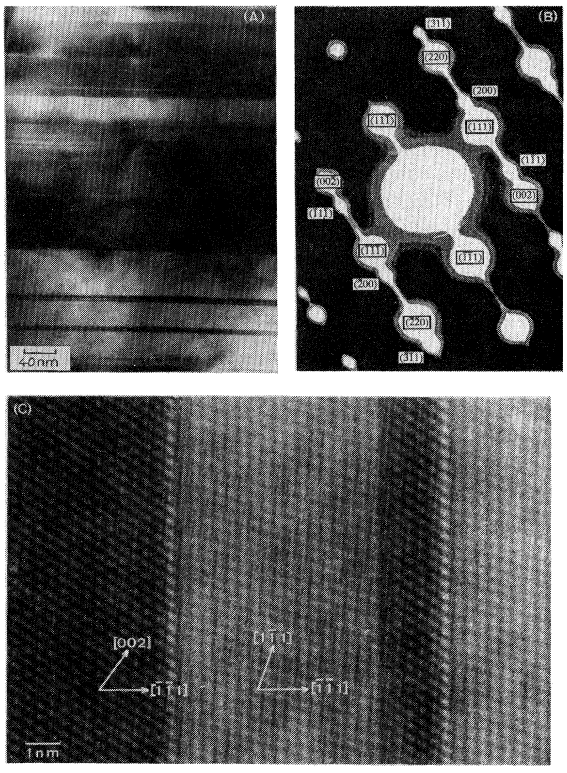

FIG. 7. Transmission electron microscopy of a sample taken to 17 GPa. (a) Low magnification micrograph showing twin planes between untransformed (dark) and transformed (light) regions. (b) Selected area electron diffraction on a zone 3 μm in diameter. Double spots are characteristic of twinned material. Common planes of the twinned crystals belong to the $[\bar{1}\,\bar{1}1]$ family. (c) High-resolution micrograph of transited (clear) and untransited (dark) regions. $(\bar{1}\,\bar{1}1)$ twin planes are normal to the plane of the figure and extend 5 to 8 nm in this direction, as calculated from the contrast.

clue to the origin of the large hysteresis of the transition and its sluggishness. Examination of the layered transformed regions reveals no faults, such as steps, at the (111) interfaces. This means that the propagation of the instability, which is easy in the (111) plane, is almost impossible normal to the plane: There are no seeding centers to start it in the ⟨111⟩ directions. The large (17%) volume decrease in a transited region relieves random internal strains in the neighboring untransformed layers, and suppresses whatever strain-induced low-symmetry regions might have been present, to start the transition on. The layered structure observed here must have lower symmetry than cubic, that is, rhombohedral or lower (e.g., tetragonal, orthorhombic, etc.). The total stress on untransformed layers has biaxial components when the transforming regions "soften" under a 17% decrease in volume. Thus the untransformed domains undergo uniaxial strain in ⟨111⟩ directions, among others, and no longer retain exact cubic symmetry. They tend towards a wurtzite-structure-like or lower symmetry. Whether or not this is quantitatively noticeable, as regards the free energy and the local transition pressure, is obviously a matter of speculation, but *stricto sensu,* the GaAs-I→GaAs-II transformation, when it actually occurs, is *not* between a cubic low-pressure phase and a high-pressure one. It is between a structure which is distorted from the zinc-blende-structure to a high-pressure phase which is more or less distorted from orthorhombic. Thus strictly speaking, there may not be a low- to high-pressure phase-boundary line in the P-T diagram. Incidentally, this type of planar defect, the structure of which is remarkably simple and the properties of which can be calculated, might be an interesting object to test two-dimensional defect and disorder theories against experiment since their fabrication is straightforward. It is worth noting here that this type of planar defect had been proposed[9] before to explain the absence of some lines in the x-ray-diffraction spectrum of GaAs-II, just above the phase transition at 21 GPa. The observed texturing was assigned to planar defects analogous to those which we report here, although possibly in a different crystal direction.

IV. X-RAY-ABSORPTION MEASUREMENTS

The oscillatory part of the x-ray-absorption edge of solids just above the energy of core-electron transition from the K, L, or M levels is caused by interference between the outgoing photoelectron and those which are backscattered by neighboring atoms. Thus both the x-ray-absorption near-edge structure (XANES) and the extended x-ray-absorption fine-structure (EXAFS) spectra contain rich information about the environment of the absorbing atom. Among others, the number of nearest neighbors and their distance can be extracted by a proper processing of the spectra. Thus x-ray absorption is quite well suited to the study of atomic rearrangement, at phase transition.

A. Experimental part

1. Apparatus

The experiments were performed at the energy-dispersive XAS station of Double Collisionneur dans l'Igloo (DCI), at Laboratoire pour l'Utilisation du Rayonnement Electromagnétique (LURE) (Orsay, France). Characteristics of this spectrometer[28,29] are the use of an elliptically bent silicon crystal as a monochromator, and of a diode array as a position-sensitive detector. With this setup, the beam can be focused down to 400 μm in the horizontal plane. In the vertical direction, the beam is limited by slits. The energy distribution within the polychromatic image of the source has a high degree of homogeneity. At the Ga K edge (10.367 eV) which was used here, an energy range of 400 eV above the edge is accessible. The same diamond-anvil cell and luminescence scale were used as in Sec. II. Several runs were performed on fine-grained powdered GaAs with silicone oil as a pressure-transmitting medium in the stainless-steel gasket hole, which was 300 μm in diameter and 80 μm thick at the start of the experiment.

2. Analysis of the data

The oscillatory part of the absorption coefficient is due to interference of the extracted electron with the backscattered waves from neighboring atoms and is given by

$$\chi(k)=\frac{\mu(k)-\mu_0(k)}{\mu_0(k)}\ , \tag{2}$$

with μ_0 the atomiclike cross section and μ the measured one. To compare data at different pressures, the spectra are normalized by setting $\mu_0=1$ in the energy range of the EXAFS measurements. In a one-electron single-scattering approximation where the wave function associated with the photoelectron is a plane wave, the absorption is given by

$$\chi(k)=-\sum_j \frac{N_j}{kR_j^2}|f_j(k)|\sin[2kR_j+\psi_j(k)] \times\exp(-2\sigma_j^2k^2)\exp[-2R_j/\lambda_j(k)]\ , \tag{3}$$

with N_j the number of neighboring atoms at a distance R_J, $|f_j(k)|$ the backscattering amplitude, $\lambda(k)$ the electron mean free path, $\psi_j(k)$ the phase shift due to both the backscattering and absorbing atoms, σ_j^2 the mean-square displacement between the absorbing atom and the jth scattering atom (Debye-Waller factor).

The photoelectron wave vector is then

$$k=\hbar^{-1}[2m(E-E_0)]^{1/2}\ , \tag{4}$$

with E the energy of the incident photon, E_0 the threshold energy.

The phase shift and the backscattering amplitude are extracted from ambient-pressure spectra where the structure and the atomic distances are known. These two quantities are taken not to vary significantly under pressure. R_j's and σ are then deduced from experimental spectra under pressure, as described in previous work.[30]

B. Results and interpretation

Figure 8 shows the XANES part of the x-ray-absorption spectrum at the Ga K edge for pressures up to

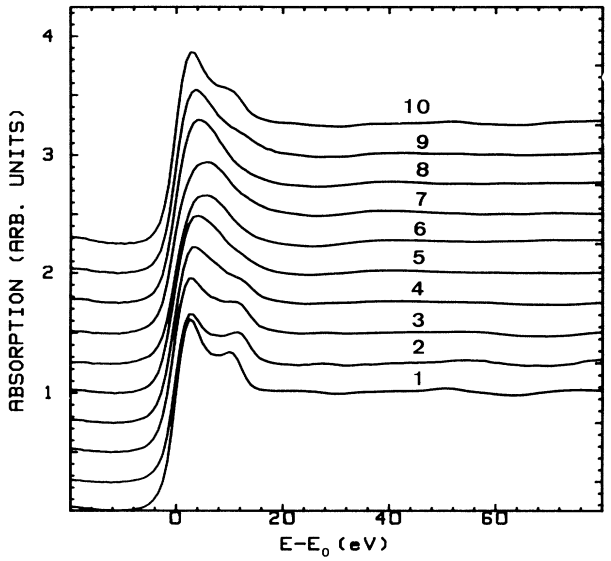

FIG. 8. Near-edge absorption spectra at the Ga K edge. $E_0 = 10\,367$ eV. Pressures in GPa are, for curves 1 to 7 on the upstroke, and 8 to 10 on the downstroke, as follows: 1, 1.2; 2, 14.8; 3, 16.4; 4, 17.4; 5, 18.4; 6, 23.7; 7, maximum pressure, 32.4; 8, 7.7; 9, 6.2; 10, ambient.

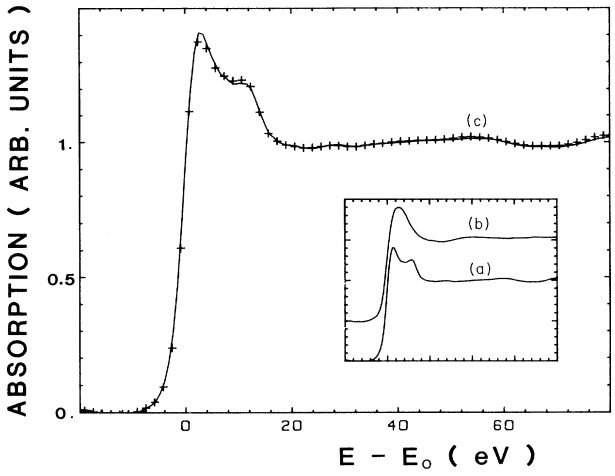

FIG. 9. XANES spectrum of GaAs at 16.4 GPa on the upstroke. The experimental spectrum (curve c, crosses) has been reconstructed (solid line) by contributions from 80% tetrahedral zinc-blende-structure GaAs at 14.8 GPa (curve a, inset) and 20% sixfold-coordinated GaAs at 23.7 GPa (curve b, inset). The fit shows that, at 16.4 GPa, 20% of the Ga sites are in a sixfold-coordinated pattern.

32.4 GPa and back. Even before making a full analysis of the spectra, the difference between cubic fourfold-coordinated GaAs-I (spectra 1, 2, and 10) and orthorhombic sixfold-coordinated GaAs-II and GaAs-III (spectra 6 and 7) is obvious. Other spectra actually represent mixed-coordination two-phase systems as discussed below. It should be noted here that XAS will not distinguish the $Imm2$ space group of GaAs-II from the $Pmm2$ space group of GaAs-III since nearest neighbors of Ga are very similar in both orthorhombic unit cells. From now on, the two orthorhombic structures will be treated together.

XAS tests the local environment of Ga atoms, that is, whether they have fourfold coordination (four nearest arsenic atoms) or sixfold coordination (four arsenic atoms plus two gallium atoms). It therefore gives a statistical photograph of the sample as regards the number of atomic sites in one configuration or another. Since these spectra are normalized, it is possible to make a weighted summation of the contributions to the total absorption of the Ga atoms in the tetrahedral and octahedral configurations. Figure 9 shows an example of such a combination: The spectrum of GaAs at 16.4 GPa on the upstroke has been reconstructed by fitting it with contributions from 80% GaAs-I at 14 GPa and 20% GaAs-II at 23.7 GPa, those two spectra being taken as being reasonably close to the one-phase spectra. In this way the evolution of the relative proportion of the low- and high-pressure phases can be followed at all pressures on the upstroke and downstroke. This can be plotted in a different manner by extracting the Ga-As distance from the EXAFS data as shown in Fig. 10. The Ga-As distance is the real bond length in cubic zinc-blende-structure GaAs-I. In GaAs-II (and GaAs-III) four Ga-As distances are mixed with two Ga-Ga distances and the data represent an average value of the distances of Ga to its six nearest neighbors. The increase of Ga-As distance at the transition is due to the increase of coordination from 4 to 6, which overcomes the 17% volume decrease at the transition. The lower and upper loci of points are the $d_{\mathrm{GaAs}}(P)$ equations of state for both varieties of GaAs. The local compressibilities are noticeably lower in the high-pressure phase than in the low-pressure one. In the transition region, the average nearest-neighbor distance varies in a continuous fashion, and this represents the gradual variation of the relative number of fourfold- and sixfold-coordinated Ga atoms. The dash-dotted line which is the bisector is arbitrarily labeled "50%" only to indicate that, at that stage, zinc-blende-structure and orthorhombic GaAs are in comparable proportions. An accurate determination cannot be made by simple interpolation and requires an adequate fit of the parameters, as shown for instance in Fig. 9, at 16.4 GPa, which is indicated as A on Fig. 10. Comparing these two results, we estimate the start of the I→II transformation (or rather of the 4→6 coordination evolution) to be close to 15 GPa on the upstroke. Along the same rules, the successive steps are as follows.

(i) 22±1 GPa, end of transformation to GaAs-II on the upstroke.

(ii) 9±0.5 GPa, start of reverse transformation on the downstroke.

(iii) 5.5±0.5 GPa, end of reverse transformation.

C. Conclusions on XAS measurements

Contrary to previous sections, this one deals with complete transformation of GaAs-I to GaAs-II and GaAs-

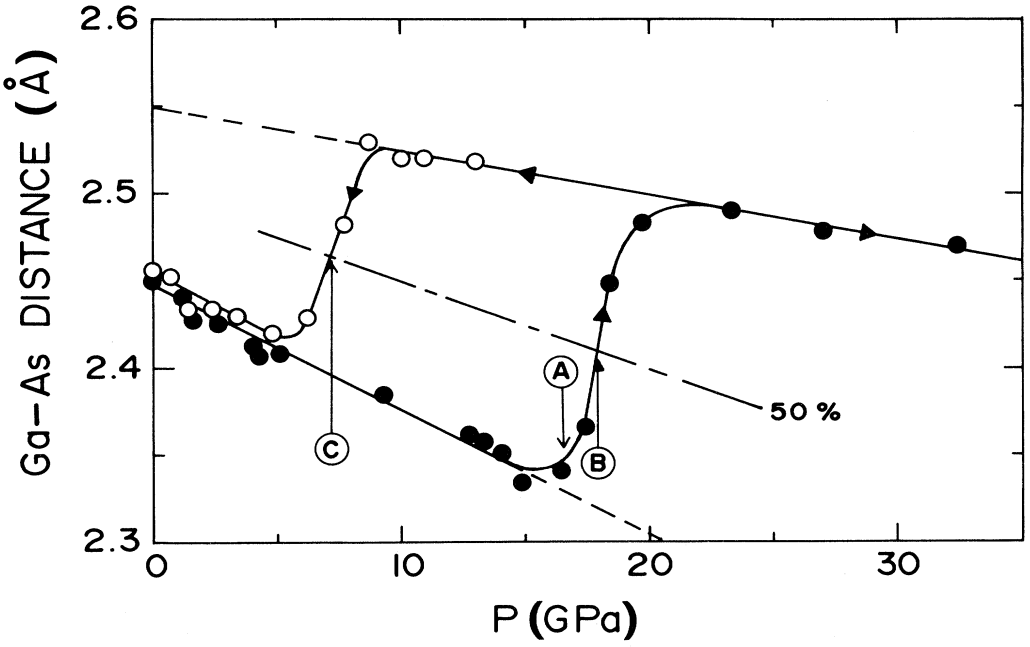

FIG. 10. Ga-As distance vs pressure calculated from EXAFS spectra using Eq. (3). Closed circles, upstroke. Open circles, downstroke. *A*, 20% sixfold-coordinated Ga atoms (see Fig. 9). *B*, approximate location of the midpoint of the transformation from fourfold to sixfold coordination on the upstroke, and *C*, on the downstroke.

III. This was done to investigate the extreme hysteresis, by not allowing any cubic GaAs seeding sites to remain in the sample. The rather large hysteresis of this transformation is obvious since between full transformation to GaAs-II to completion of the reverse one, that is from 21 to 5.5 GPa, there is an interval of some 16 GPa. If one were to take the old and classical rule for locating phase transitions, that is at the midpoint of the hysteresis cycle, points *B* (~18 GPa) and *C* (~8 GPa), we would find $P_T = 13$ GPa, or rather $P_T \leq 13$ GPa since the reverse transition is in disordered material and must have less hysteresis than on the upstroke where well-ordered material is transformed. Since no GaAs-I recrystallization seeds were left at high pressure, the reverse transformation starts at a lower pressure (9 GPa) than in incompletely transformed samples ($P_{max} < 20$ GPa), as will be shown in the next section.

V. RAMAN SCATTERING

The methods which have been described up to the present point have yielded mainly structural information about GaAs at the various stages of the transition that is, occurrence of diffusing phase-II clusters (Sec. II), geometry and size of the precursory defects (electron microscopy), and partial transformation to amorphous GaAs on the downstroke (Secs. I and III). Little else can be derived on the physical parameters such as electronic structure or interatomic restoring forces, with the obvious exception of the evolution of the band structure of phase I (Fig. 1).

Raman scattering is a powerful method because it incorporates both electronic properties (resonances) and vibrational properties (phonons). Moreover, selection rules give information on the symmetry—or lack of symmetry—of the crystal. The shift of the eigenfrequencies of the lattice in microcrystals also gives an estimate of their size. Finally, in imperfect crystals, defect sites may give rise to localized or resonance modes, or defect-activated Raman modes.

A. Experimental part

The samples were the same (100) slabs as described in Sec. II. The pressure-transmitting fluid was an ethanol-methanol mixture. The cell was a membrane diamond-anvil cell[31] (MDAC) where pressure can be varied by pneumatic bellows. The pressure was evaluated with the ruby scale as in Sec. II but, above 10 GPa we used, in addition, the LO and TO frequencies of the zinc-blende-structure lattice as an internal pressure gauge. Around 20 GPa, the pressure in the ethanol-methanol medium, where several ruby chips had been dispersed, proved to be inhomogeneous enough as to vary by over 1 GPa from one part of the cell to another, especially after the 17% volume decrease at the phase transition which grossly perturbs the stress configuration within the cell. The spectrometer was an *XY* 1000 Dilor system, used in the double monochromator optical multichannel analyzer (OMA) mode, in the backscattering geometry. The 514.5-nm ($h\nu = 2.409$ eV) line of an argon laser was used at powers of 5 mW, when the sample was outside the cell. The laser spot was 20 μm in diameter. In the cell, a power of 50 mW incident on the diamonds proved to be low enough not to cause any heating of the sample in the pressurizing medium. This was verified by varying the

incident power and observing that neither the Stokes to anti-Stokes intensity ratio nor the frequency of the LO mode varied within experimental precision. The location of the laser spot on the sample on the Dilor spectrometer mount could be monitored and reliably reproduced within 5 μm and with the MDAC the pressure was pneumatically varied[31] without any misalignment. Thus the Raman results given here actually are a set of measurements on various well-localized regions of the sample.

B. Results and analysis

1. Upstroke

The variation of the LO and TO modes is shown in Figs. 11(a) and 11(b). Since the TO is forbidden in this geometry, it becomes more easily observable by resonance around 10 GPa or so (Fig. 12) when the laser energy (2.409 eV) becomes comparable to that of the direct gap (cf. inset in Fig. 1). The lower part of the diagram of the LO frequency versus pressure, that is below 10 GPa where pressure is homogeneous in the cell, is taken as the internal pressure gauge for the sample. The pressure dependence of both modes has been fitted with

$$\nu_{LO}=291.6+3.8P-0.013P^2 ,$$

$$\nu_{TO}=266.4+4.22P-0.015P^2 ,$$

with ν in cm^{-1} and P in GPa.

The intensity of both LO and TO modes has a resonance with a maximum in-between E_Γ^d and $E_\Gamma^d+h\omega_{phonon}$, as expected[32] (ingoing and outgoing resonances). A noteworthy feature is that the ratio of LO to TO intensities is not symmetrical with respect to the resonance. It should be, within the small (25 cm^{-1}) difference in energy of the two modes. This means that in the region of 15 GPa, the crystal is already perturbed enough to allow selection rules to be broken through local structural defects and/or crystallites' misorientation. Secondly, the steepness of the decrease in intensity above 14 GPa is to be related to diffusion on the incident and outgoing light as was shown in transmission in Sec. II. Finally the sharp decrease around 16 GPa marked by an arrow in Fig. 12 just locates the pressure where the crystal irreversibly becomes opaque at the transition.

2. High-temperature measurements

The temperature of the sample can be varied *in situ* by increasing the power of the laser. The temperature of the

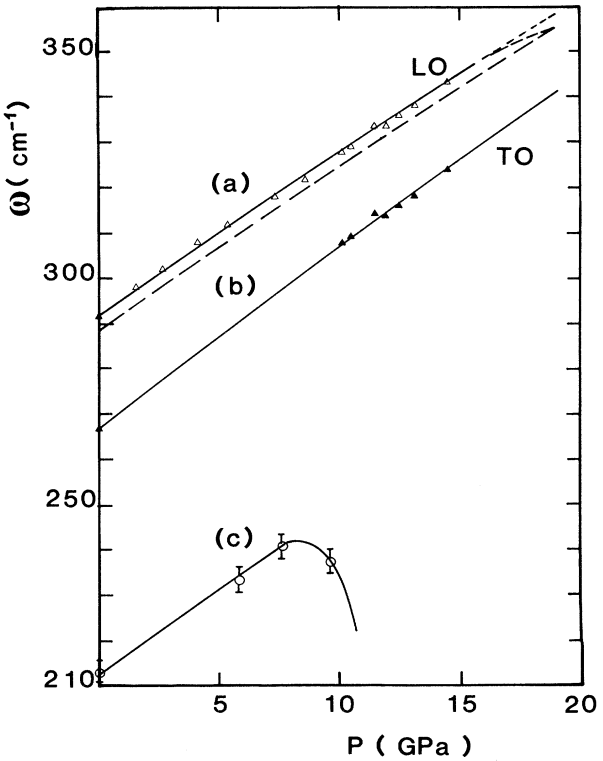

FIG. 11. Raman wave number of observed modes vs pressure. (a) Open triangles, solid line, LO phonon at increasing pressure. Dashed line is shifted down by ~ 3 cm^{-1}, on the downstroke, to reproduce the disorder-induced shift observed at ambient pressure (see Table II). (b) Closed triangles, TO mode. (c) Open circles, pressure dependence of the defect-induced A feature (cf. Sec. V B 3) observed on the downstroke, after the transition.

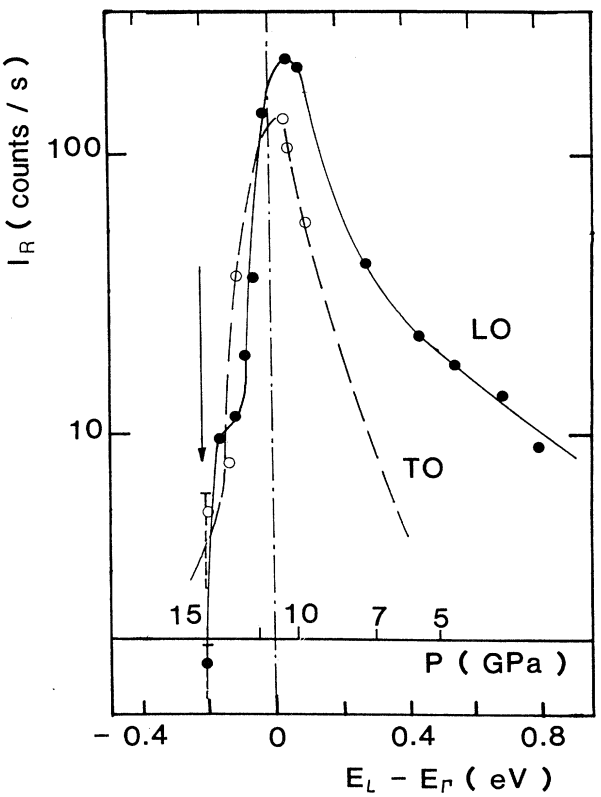

FIG. 12. Raman intensity of the LO (closed circles) and the TO (open circles) modes on the upstroke, at constant incident laser power. Lower abscissa scale, energy difference between the laser light ($E=2.409$ eV) and the direct gap energy (E_Γ). E_Γ is related to pressure (upper abscissa scale) as shown in the inset of Fig. 1. The sharp decrease in intensity (arrow) above 16 GPa shows the opacification of the crystal due to the transition.

active region of the sample can usually be determined by the ratio of the Stokes to anti-Stokes intensity or be derived by measuring the shift of the Raman line, the temperature coefficient of which is,[33] in the zinc-blende-structure phase,

$$d\nu/dT = 0.016 \text{ cm}^{-1}\text{K}^{-1} .$$

In the range of pressure of interest here (< 15 GPa), the first method is inapplicable since the resonance on the Raman cross section, the intrinsic absorption and reabsorption processes at the direct- and indirect-gap transition energies, and the diffusion which precedes the phase transition completely throw off the Stokes to anti-Stokes intensity ratio. The shift in energy of the TO mode relative to 300 K was used as a temperature gauge and a sharp decrease of the intensity with increasing temperature showed the transition to occur at 620±20 K, at 13.6 GPa.

3. Downstroke

Incompletely transformed samples ($16 < P_{\max} < 18$ GPa) which are studied in this section only show very weak LO and TO modes between the maximum pressure and ~10 GPa. Below this pressure, additional features appear which are shown in Fig. 13 for a pressure of 7 GPa. The wave-number shift with pressure of the main feature, *A* in the spectrum, is compared with the pressure dependence of the LO and TO modes in Fig. 11(c). The intensity of this peak reaches a maximum in the vicinity of 7 GPa, and almost disappears at a few gigapascals above ambient. Its pressure coefficient below 8 GPa is very similar to that of the lattice modes: 3.5 $\text{cm}^{-1}\text{GPa}^{-1}$.

At ambient, retrieved crystals were studied outside the DAC [Fig. 14(a)] and annealed at high temperature. Recrystallization of the sample is evident in Fig. 14(b), although the high intensity of the TO mode, which was forbidden in the original (100) geometry [Fig. 14(c)] bears testimony to the high degree of orientational disorder that remains in the sample after the phase transition. Also, the LO mode is some 3 cm^{-1} lower in energy than in the unperturbed crystal. Those two points will be discussed in Sec. V C in relation to the size of the crystallites created by the phase transition.

C. Discussion

Several features observed in this section require specific discussion and/or interpretation.

1. Variation of the LO mode as a pressure gauge

The use of the pressure variation of the LO phonon as a pressure gauge deserves some comment. In the higher-pressure range (12–20 GPa), ethanol-methanol mixture is known to be a stiff glass and pressure gradients in the medium are readily observable when several ruby samples are put at different locations in the cell, as in our experiments. On the upstroke up to ~15 GPa these differences were tolerable, that is, less than 1 GPa. At the transition,

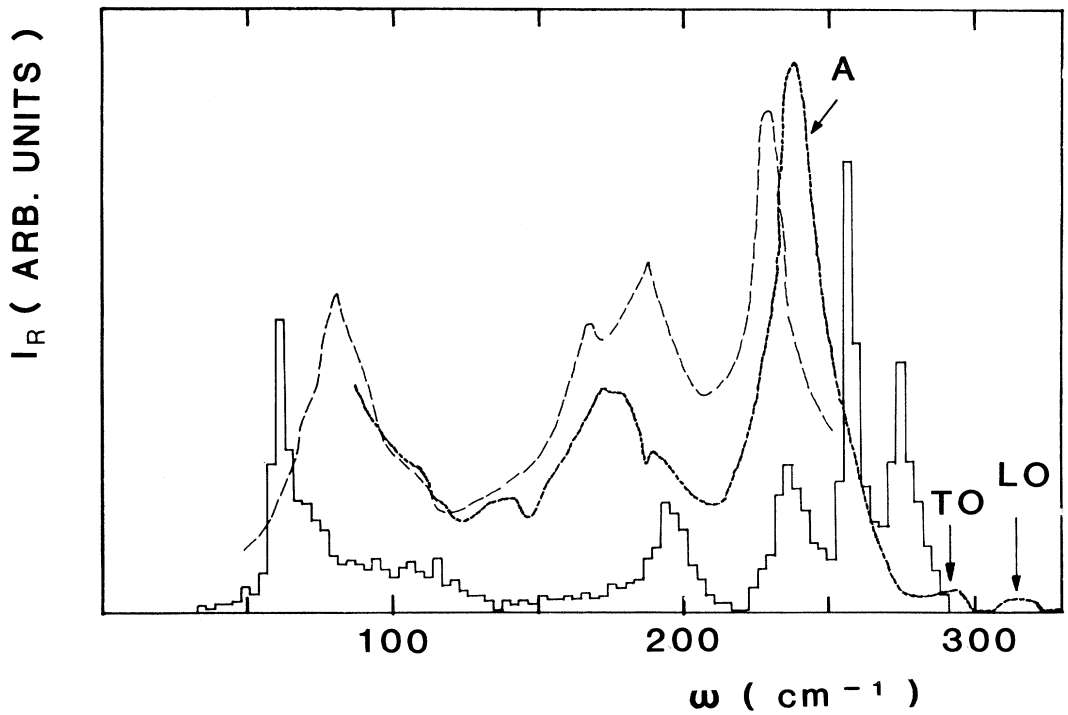

FIG. 13. Comparison of the Raman spectrum of GaAs, at 7 GPa, on the downstroke from 18 GPa (dotted curve, feature *A*), with electron-irradiated GaAs (Ref. 36) at ambient pressure (dashed curve). Stepped spectrum is the density of states of GaAs at ambient (Ref. 37). LO and TO arrows point to the optical modes of the zinc-blende-structure fraction of the crystal.

inal pressure of ~18 GPa, although the transformed portion of the crystal was only of the order of 20–50 %, the corresponding volume collapse (4–10 % possibly) was enough to increase the gradients within the ethanol-methanol mixture to over 1 GPa. Correspondingly the apparent pressure in the crystal, as calibrated by extrapolation of the upstroke $\nu_{LO}(P)$, was lower by 1 or 2 GPa. There are two reasons for this.

(i) The crystal is indeed at a lower pressure after shrinking down to denser GaAs-II, in its stiff environment.

(ii) It has crumbled down to microcrystallites as shown by the ~3 cm^{-1} overall decrease of the LO frequency, on the downstroke, in the region between 10 GPa and ambient where ruby pressure readings are reliable. Now this decrease of the LO frequency can be assigned to well-documented size effects and, as will be shown in Sec. V C 3, the sample at ambient is composed of 5–10 nm disoriented crystallites. It is only reasonable to assign their origin to the state of the crystal at its maximum pressure. Since GaAs-I is still largely present, and thus metastable at 18 GPa, it has no reason to crumble to smaller crystallites on the downstroke. Thus the conclusion is as follows: The size effect on the LO frequency should be about constant all the way from maximum pressure down to zero and we drew the dashed $\nu(P)$ curve in Fig. 11 on the downstroke along this assumption. We do have a problem in the upstroke region between 16 and 18 GPa, since we do know the crystal has started disorienting but we cannot evaluate the crystallites' size. To solve this problem, we also used the pressure dependence of the TO mode which was found to be much less sensitive to size effects ($\Delta\nu < 1$ cm^{-1}) as an auxiliary gauge on the downstroke where disorientation fortunately makes it allowed and intense.

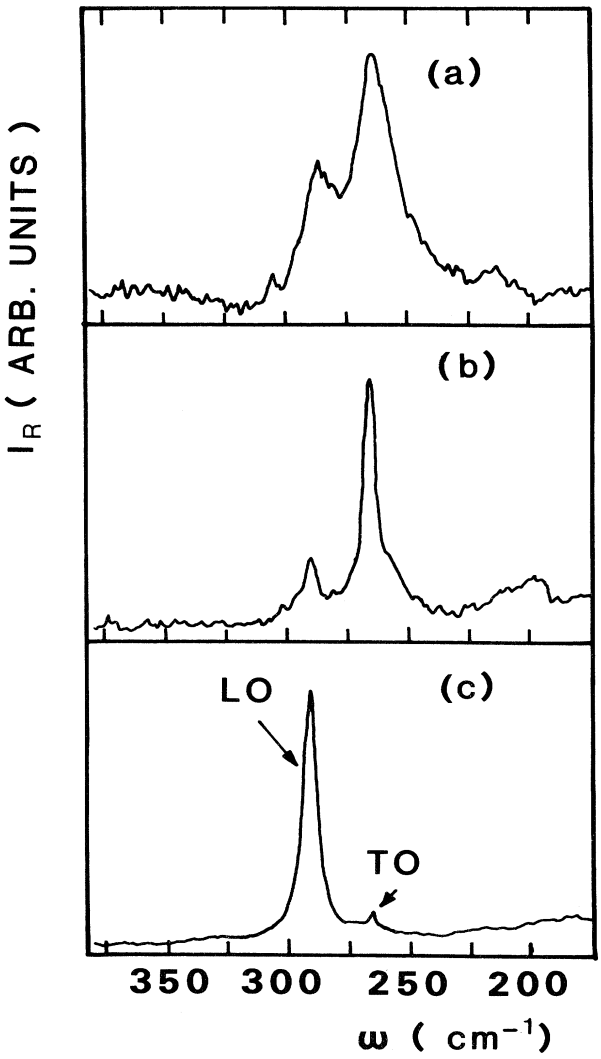

FIG. 14. LO and TO modes of pressurized samples. (a) 300 K, ambient pressure after pressurization to 18 GPa. (b) Same after annealing of the pressurized sample at 850 K. (c) Initial spectrum of the original [100] slab before pressurization.

2. *Raman scattering from defects*

The origin of the scattering observed in Fig. 13 evidently may be traced back to some kind of pressure-induced defect rather than to a new phase.[34] In the present discussion we shall concentrate on the evolution of feature A, that is, the main peak, because the other features are broader and weaker, although present at all times, and also because the experimental setup did not allow easy observation of the low-energy ($\nu < 100$ cm^{-1}) part of the spectrum where other features may be present. Such defect-related features have been induced previously by alloying.[35] But since we are dealing here with pure GaAs, it is only natural to compare with defects which do not introduce host atoms such as those created by electron or neutron bombardment.[36] In Fig. 13, the dashed line shows such a comparison with samples having an estimated 5×10^{17} cm^{-3} defects created[36] by 1.6-MeV electrons. The curves are similar, although shifted down in frequency. The defect-induced spectrum is shown here at 7 GPa. Using the LO and TO intensities as a common gauge, we can estimate the defect density to be ~10^{19} cm^{-3}. Another possibility would be to assign this feature to an amorphous part of the sample. But in this case we would expect it to be much weaker than the LO and TO modes, which is not the case, as shown in Fig. 13. Besides, the shape of the spectrum itself is quite different from that of amorphous GaAs.[37]

We will thus adopt the conclusions[36] of Berg and Yu, that these defects are arsenic vacancies. This is confirmed by the fact that our ambient-pressure annealing of the samples makes the peak disappear at 300 °C which fits with the arsenic-vacancy annealing temperature. Thus the intensity of the A peak versus pressure will be taken to represent the concentration of As vacancies in fourfold-coordinated GaAs. It is a signature not only of the As vacancy, but also of the coordination of its environment. Defects in sixfold-coordinated GaAs would have a different—presumably much lower—frequency. We noted before that those defects appear around 10 GPa, increase in number at ~7 GPa, and

disappear at ambient. How does this fit with the previous conclusions on the reverse transition process? We know that around 10 GPa (EXAFS), gallium atoms start changing back from coordination 6 to 4. We must remember that the present XAS experiment tests only the environment of Ga atoms. Now this coordination change is a gradual process and certainly has to proceed through unstable local atomic configurations before reaching the stable fourfold-coordination arrangement. For instance, a sixfold-coordinated Ga atom will lose an arsenic site and be surrounded by five atoms only when the local orthorhombic symmetry tends to cubic. It is equivalent to a Ga atom close to an interstitial. Thus a pair of neighboring Ga atoms may find themselves in a cubic environment with five and three As nearest neighbors instead of four and four. This is a vacancy-interstitial pair which will anneal when complete fourfold coordination is restored. Thus this type of defect is a channel through which the sixfold coordination can transform into the fourfold coordination. As expected, when this process is at its maximum (~ 7 GPa) the "speed" of the transformation, that is the slope of the downstroke curve on Fig. 14 (point *C*), is maximum. Of course, at room temperature, vacancy migration is strongly impeded and this process leaves behind a strong lattice disorder which is analogous to amorphization, as seen before. This disorder must involve Ga—Ga bonds remaining from the high-pressure sixfold-coordinated phase, which also have been shown to exist in amorphous GaAs and GaP.

3. *Annealing at ambient pressure*

The LO and TO modes on the retrieved material [Fig. 14(a)] are visibly different from the original ones [Fig. 14(c)]. Apart from the activation of the forbidden TO by crystal disorder, the modes are broadened and shifted and this evolves with annealing at ambient pressure as shown in Table II. From the broadening and the shift of the modes, we can now proceed to evaluate the average size of crystallites. This has been done in several papers[35,37] by noting that the correlation length L of optical phonons will be limited by crystallite size and thus selection rules will be lifted over a wave-vector interval $\Delta k \sim 1/L$. When this is a sizable fraction (a few percent) of the Brillouin zone, the downward curvature of the $\omega_{LO}(k)$ phonon branch will cause the LO-phonon peak to be broadened and shifted to lower frequencies. Using this procedure[35,37] one can derive, for instance, the size of crystallites created in GaAs at different depths by ion bombardment. Using the same gauge, we find that a LO-frequency shift of -3.3 cm^{-1}, and a full width at half maximum (FWHM) increase of 5.5 cm^{-1}, correspond to crystallites 5 to 6 nm in size. This corresponds well to the order of magnitude of microcrystals in fully transformed samples ($P_{max} > 18$ GPa) as observed by electron microscopy or to that of interplanar distances that were observed in Fig. 7, that is, 5 to 10 nm. The TO phonon cannot be used as a gauge since its frequency variation is expected to be smaller. Indeed, if we remember (Fig. 7) that the phase transition is highly anisotropic in the $\langle 111 \rangle$ directions, we expect most of the broadening to occur from those of the phonons which propagate in the Λ direction. And indeed[38] in this direction the TO branch is almost flat, whereas the LO branch has a negative curvature which corresponds to $L \sim 5$ nm for a shift of 3 cm^{-1} of the LO frequency. After annealing, the line position and FWHM of the LO frequency are the same as at the start within experimental error, which indicates that the average crystallite size should be at least 50 nm or larger, after annealing.

VI. PHASE TRANSITION IN GaAs

We are now in position to discuss the transition mechanisms in zinc-blende-structure GaAs under pressure, relate the different phenomena that we observed to successive steps in this transition, and finally define the stability limits of GaAs-I and GaAs-II at 300 K, the so-called "transition pressure." For this discussion we shall distinguish between the upstroke and the downstroke. In the latter, the behavior of fully transformed samples which have been taken to pressures above 24 GPa differs somewhat from that of partly transformed samples which have been taken to pressures between 14 and 18 GPa. Their behavior is summarized in Table III. The values given for the pressures in this table obviously must be taken only as indications for the location of the successive steps of the transition, not as very precise values. We can now compare the different limits of the apparent location of the phase transition which are imposed by the various methods that we examined, as shown in Table IV, which justifies the value of 12.5 ± 1.5 GPa for the stability limit of GaAs-I which we had anticipated in Table III. A few remarks can be made regarding this value.

(1) It is imposed by the analysis of the behavior of the crystal investigated by several methods if we want to ac-

TABLE II. Full width at half maximum and location of the maximum (cm^{-1}) for the LO and TO Raman lines at ambient pressure and room temperature. First column, Fig. 14(c), original crystal. Second column, Fig. 14(a), Same crystal after pressurization to 18 GPa at 300 K. Third column, Fig. 14(b), pressurized sample after annealing at 850 K at ambient pressure.

		Untransformed crystal 300 K (c)	Transformed crystal 300 K (a)	Transformed after annealing at 850 K (b)
FWHM	LO	6.5	12	6
(cm^{-1})	TO	8	19	6
σ Raman	LO	291.6	288.5	291.3
(cm^{-1})	TO	266.4	266.5	266.7

count for all observations. It represents a region through which the line of true thermodynamic equilibrium lies, if indeed such a thing exists for this type of transition. In any case, *outside this region,* either zinc-blende-structure GaAs-I *or* orthorhombic GaAs-II is thermodynamically unstable.

(2) This analysis of the transition also accounts for other published observations, for instance, the resistivity change at ~18 GPa. A clear resistivity drop will be observed only when the percolation limit (~15%) is attained for a conducting phase (GaAs-II) dispersed into an insulating one (GaAs-I). And this implies that a *much larger* fraction of the sample (50%?) be transformed to the sixfold-coordination pattern. If GaAs-II is a semimetal or a semiconductor, small atomic clusters with sixfold coordination will not have high conductivity; semimetallic conduction also requires extended order, that is, microcrystals. And we have seen before, that at 16.6 GPa, although 20% of the crystal shows up with sixfold coordination (EXAFS), although it is optically opaque, nevertheless x-ray-diffraction patterns barely[10] start to show GaAs-II lines.

(3) Interestingly enough, this quantitative result has implicitly been in the literature for over 25 years: Using data published[2,3] in 1963 by Jayaraman, Klement, and Kennedy, we shall proceed in the next section to show, using these published data at high pressure and temperature, together with unavoidable thermodynamic constraints around the triple point, that the intersection of the GaAs-I→GaAs-II phase-boundary line with the 300-K isotherm *cannot* lie higher than 14 GPa.

TABLE III. Steps in the phase transitions of GaAs with increasing and decreasing pressure. "Partly transformed samples" refers to pressures not exceeding ~18 GPa. "Fully transformed samples" have been taken to 22 GPa at least.

Pressure (GPa)	Steps in the transformation	
	Upstroke	
12±1.5	GaAs-I unstable with respect to GaAs-II (cf. Table IV)	
13.5 to 14	Irreversible opacity sets in (Fig. 3)—Twinning planes appear	
15	Sixfold coordination sets in (Fig. 10)–Weak Debye-Scherrer lines on retrieved samples: Crystalline disorder	
16.5	Organization of orthorhombic lattice starts (Ref. 10)—Sizable fraction (~20%; Fig. 9) of atoms already in sixfold coordination	
17 to 19	Sample gradually becomes opaque and reaches full crystalline disorder—Still contains a large fraction of zinc blende (Fig. 10)	
18±1	~50% of the sample transformed to sixfold coordination—Microcrystals are a few nanometers in size	
≥22	Full transformation to orthorhombic GaAs-II or GaAs-III	
	Downstroke	
	Partly transformed samples	Fully transformed samples
12±1.5	GaAs-II Unstable with respect to GaAs-I (cf. Table IV)	
10.5	Transformed fraction starts reverting to I: Seeding from untransformed regions	Nothing happens: No GaAs-I seeds are present
10 to 9	GaAs-II reverts back to faulted zinc blende (Fig. 13)—As vacancies—Ga-Ga pairs (?)	Start reversal to fourfold coordination (Fig. 9)
7±1.5	Faulted GaAs-I anneals in part to amorphous (Fig. 5)	50% of the sample is back to GaAs-I (crystalline, faulted and/or amorphous)
5±1		End of transformation back to fourfold coordination
Ambient	Samples with $P \geq 17$ GPa are made of microcrystals with size of the order of 5 nm (Fig. 14) and variable amount of amorphouslike material depending on P_{max}	

TABLE IV. Summary of the apparent location of the phase transition in GaAs depending on the experimental method used. Hatched regions on the upstroke (right-hand side) indicate the instability region of GaAs-I as observed by the different methods. On the downstroke (left-hand side) they indicate the instability of the high-pressure phase. Dashed vertical lines thus locate the pressure domain where the thermodynamic transition point must be.

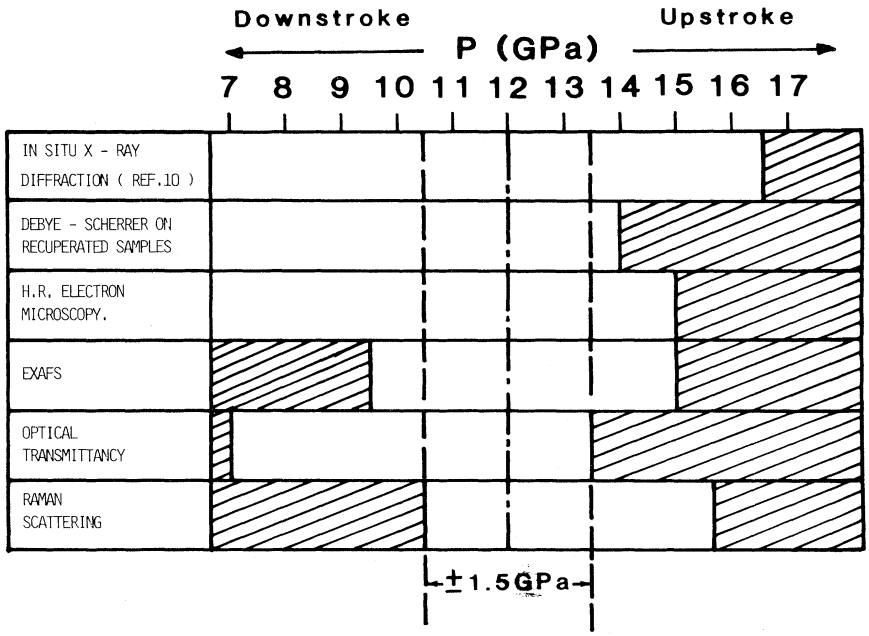

VII. PHASE DIAGRAM OF GaAs

A. Thermodynamic rules

We noted in the Introduction of this paper that the determination of the transition pressure for two structures at zero temperature was a difficult problem even if 300 K is taken to be close enough to 0 K. The former section and the lengthy analysis which was required just to get a single point on the P-T phase diagram bear testimony to this. Actually, a zero-temperature (room-temperature) isotherm in the P-T diagram of any system can be correctly derived only by consideration of the atomic positions all over the P-T plane. Atomic-position variations yield, among others, the domains of existence of various possible crystal structures (phase boundaries) and the density as a function of pressure and temperature, with the characteristic ΔV's (volume variation) at the phase-transition lines. Among others, the simple $V(P,T)$ surface, that is the molar volume, has to obey a number of thermodynamic constraints to fit with the well-determined isobars and isotherms, if any, and follow the regularities in the thermodynamic properties along the Periodic Table of Elements (Figs. 15 and 16). Here, we shall use the rules around a triple point: The volume V and entropy S variations must be zero for any closed path around it so that

$$\sum_{i=1}^{3} \Delta V_i = 0 \ , \tag{5}$$

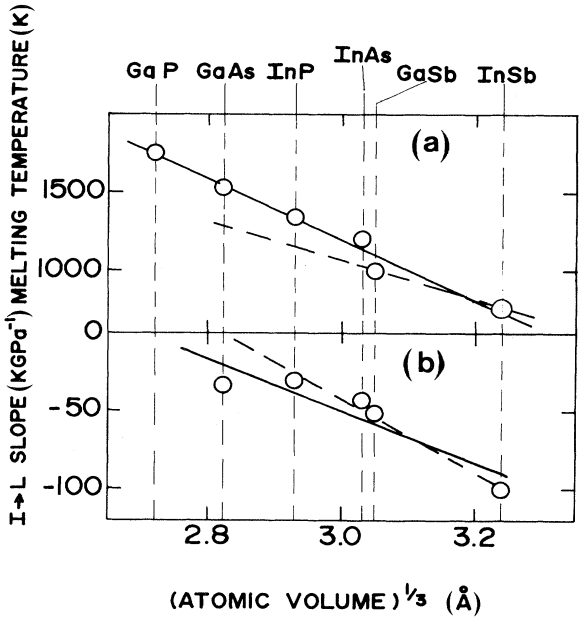

FIG. 15. Regularities in the behavior of thermodynamic quantities in the III-V semiconductor family (from Ref. 2). Melting temperatures (a) and melting line slopes (b) vs interatomic distance in this series are averaged by solid lines. Dashed lines going through GaSb and InSb still give sufficient estimate of the actual values for GaAs.

$$\sum_{i=1}^{3} \Delta S_i = \sum_{i=1}^{3} \Delta V_i \left[\frac{dP}{dT} \right]_i = 0 \ , \tag{6}$$

dP/dT being the slopes of the phase boundary lines. We shall use these relations here to derive the phase diagram of GaAs.

B. Previous work on the phase diagram of GaAs

Very little has been published on this subject. The only experimental data as noted above are those of Jayaraman on the phase boundary line between the zinc-blende solid and the liquid,[2] up to 5 GPa, and several papers reporting the ΔV's between phases I and II at 300 K, the last one being Ref. 10. Using these data and a model introducing electronegativity differences as a scaling parameter which combines the concepts of valence and size difference, Van Vechten[7] calculated the heat of fusion, melting points, and P-T phase diagrams of a variety of covalent and ionicovalent semiconductors. Unfortunately, for GaAs, as well as for other compounds, he strove to have the I→II phase-boundary line go through—or at least not too far from—the "experimental" values at 300 K. (See line labeled F in Fig. 17.) Now the slope of a phase-boundary line is, by Clapeyron's equation [Eq. (6)], $dT/dP = \Delta V/\Delta S$. Since ΔV is large and negative, a negative slope means a large positive entropy variation when going from phase I to II, that is among most of the curvaceous line F of Fig. 17. This positive entropy variation would, however, come from the vibronic contribution since the electronic part is negative and would lead to an unreasonably large decrease in the Debye temperature when going from GaAs-I to the high-pressure phase(s). In any case, the general shape of the I→II phase-boundary line, in those systems where it is known, that is InSb (Ref. 39) or in the II-VI compounds,[2] for CdS, CdSe, CdTe, and HgSe, is quite close to a straight line in the P-T plane with very large positive or negative slopes of the order of ± 1000 K GPa^{-1}. There is no experimental example of the behavior suggested by Van Vechten for the I-II phase boundary, such as curve F in Fig. 17. Thus in Sec. VII C, we shall reconstruct the GaAs phase diagram assuming all three phase boundaries to be straight lines throughout, as is the case, to a tolerable approximation in all known III-V and II-VI compounds.

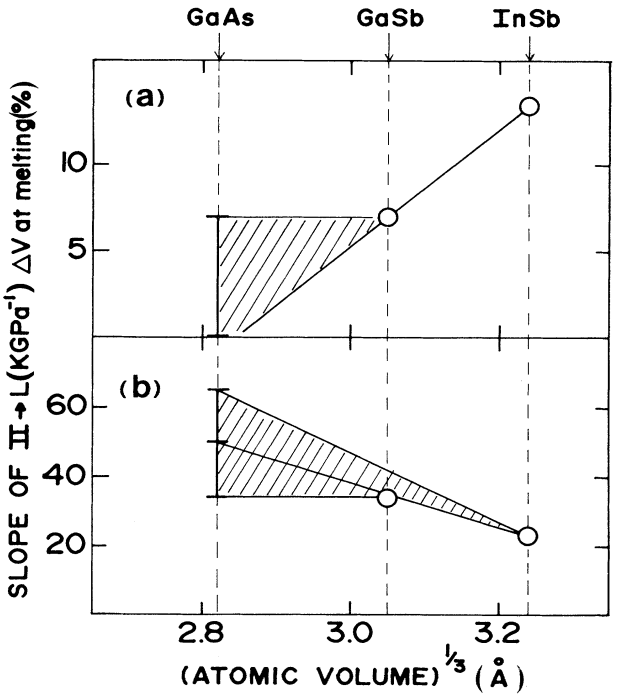

FIG. 16. Estimate of the volume variation at melting (a) and of the melting slope of the high-pressure solid (b) for GaAs, by extrapolation from GaSb and InSb. Hatched regions indicate the limits of our extrapolation. Note that the uncertainty we tolerate here is much larger than the observed deviation between solid and dashed lines in Fig. 15.

C. Construction of the diagram

The only data we have for GaAs are the I→L (zinc-blende structure to liquid) slope[2] which is -34 K/GPa and the volume variation at the I→II phase transition which has been measured by a number of authors, the latest value[10] being $\Delta V = -17.2\%$.

We thus have to determine (i) The location of the triple-point pressure and temperature, (ii) the ΔV's for the I→L and II→L melting lines (L, liquid) and (iii) the slope of the II→L melting line.

1. Location of the triple point

Although quite a few predictions in Van Vechten's model did not compare well with experiment, one remarkable feature is that it *does* predict the triple-point temperatures T_t within 40 K in all cases where experimental data exist, that is Si, Ge, GaSb, and InSb. Thus we take for T_t of GaAs his computed value of 1010±40 K. His model is far less successful in predicting the triple-point pressures P_t. In GaSb and InSb, it is too high by some 2 GPa. Thus his value of 12.5 GPa for GaAs should probably be taken down to 10.5 GPa. We shall therefore take $10.5 < P_t < 12.5$. This defines the rectangle in Fig. 17. Finally the triple point must lie on the I→L phase-boundary line with a slope of -34 K GPa^{-1} which leaves us, for the best compromise for the location of the triple point, with $T_t = 1050$ K; $P_t = 12.5$ GPa. It should be understood that this is an extremal value. If the I→L phase-boundary line were to bend down as indeed it does[2] in GaSb, P_t would be even lower, and that would strengthen the point that we are making here.

2. Slope of the II→L line and ΔV's at melting

To derive these quantities, we shall rely on the regularities in the thermodynamic properties of III-V compounds along the Periodic Table. These regularities have been recognized for a long time[2] and, before going further, two examples are given in Figs. 15(a) and 15(b), for the melting temperatures and melting line slopes of six III-V semiconductors. This is plotted versus mean in-

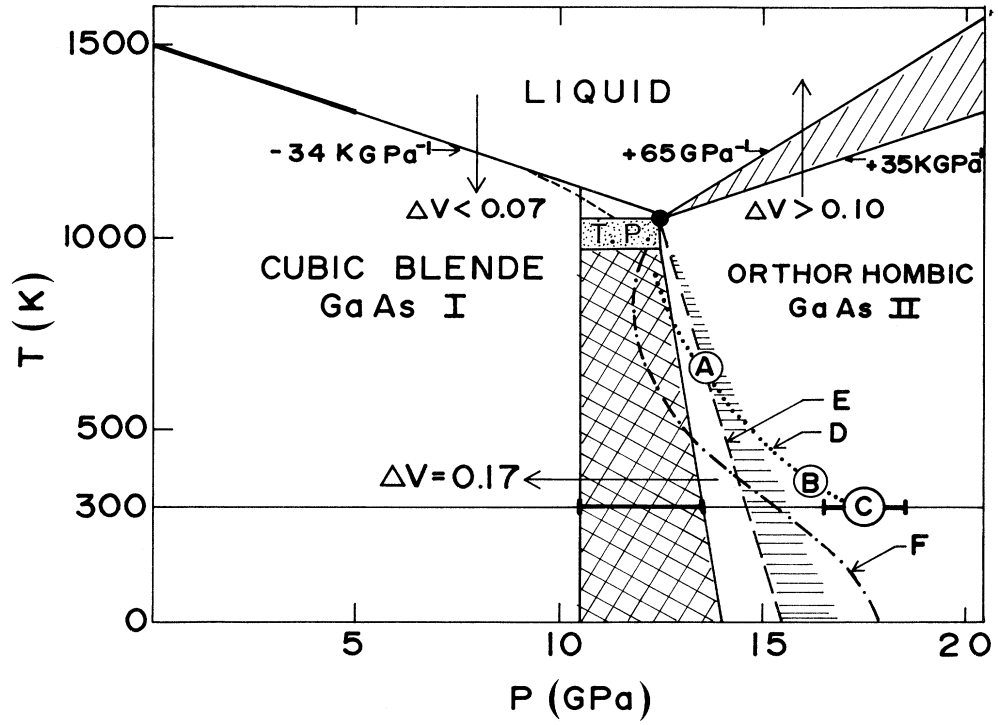

FIG. 17. Phase diagram of GaAs. T.P. in dotted rectangle, location of the triple point (see text). Crosshatched area, location of the "phase-boundary line" between low- and high-pressure GaAs. This is limited, on the 300-K isotherm, by the heavy line extending along 12±1.5 GPa. The meaning of this delimitation actually is as follows: on its right, zinc-blende-structure GaAs is thermodynamically unstable; on its left, GaAs-II is unstable. Dotted line *D*, "Full" transition to GaAs-II on the upstroke (see text), joining *A*, *B*, and *C*. *A*, our high-temperature measurement; *B*; Ref. 16; *C*, published values in Ref. 19. Dashed line *E*, extreme right-hand limit for the phase boundary (Sec. VII C 3). Dash-dotted line *F* from Ref. 7. Melting line slopes and ΔV's as explained in text. Heavy section on the I→*L* melting line from Ref. 2. Dashed line is to illustrate that if the melting curve bends down, as it does in other cases, this will only bring the location of the triple point to lower pressures.

teratomic distance, that is, (atomic volume)$^{1/3}$, which is the relevant parameter here. The regularity of the trend is obvious. Now for the other quantities, we only have data for GaSb and InSb and it may seem farfetched to extrapolate for GaAs just from those two points. Actually, we do not need accurate values at all. The only thing we need to note is that the trend is regular: There is no change in slope when going from GaAs to GaSb to InSb. A straight line through the GaSb and InSb data gives an approximation of the relevant quantity for GaAs which is more than sufficient for our purpose.

We shall now determine $[dT/dP]_{II\to L}$ and $\Delta V_{I\to L}$. The ΔV at melting for GaAs-II will just be the complement to 17.2% to the former. Figure 16 shows the result. In Fig. 16(a), we see that extrapolation gives $\Delta V_{I\to L}=0$, which is the lower bound. The upper is $\Delta V_{I\to L}=7\%$. In Fig. 16(b), the GaSb-InSb straight line extrapolates to about 50 K GPa^{-1}. The lower bound in this case is the value for GaSb, i.e., 34 K GPa^{-1}. For the upper bound, we took a symmetric value, which is surely quite overestimated, giving an estimate of

$$34<[dT/dP]_{II\to L}<65 \text{ K GPa}^{-1} .$$

It must be noted that applying those error estimates to Fig. 15 does show that actual GaAs data would indeed be within the extrapolations. The limits for the last quantity, that is $\Delta V_{II\to L}$, are simply the complement to 17.2% of $\Delta V_{I\to L}$, that is, $10.2\%<\Delta V_{II\to L}<17.2\%$.

3. *Zinc-blende-structure orthorhombic GaAs phase line*

We are now in a position to evaluate the limiting value of dT/dP for the I→II phase-boundary line, by calculating $\sum\Delta S=\sum\Delta V(dP/dT)=0$. We take the ΔV's to be constant, even $\Delta V_{I\to II}$. If anything, it should increase in going from 300 K to the triple point, and this would only move the phase-boundary line towards lower pressures, which only helps make our point. For simplicity, we express the ΔV's in percent of the GaAs-I molar volume although it does somewhat vary in the *P*-*T* plane. Thus with

$$[dt/dP]_{I\to L}=-34 \text{ K GPa}^{-1} , \quad \Delta V_{I\to II}=-17.2\% ,$$

the entropy conservation relation reads

$$-\frac{\Delta V_{L\to I}}{34}-\frac{17.2}{X}+\frac{17.2-\Delta V_{L\to I}}{(dT/dP)_{II\to L}}=0. \tag{7}$$

X, the solid-solid transition line slope, is a function of two variables: $\Delta V_{L\to I}$, which may vary between 0 and 7%; and $(dT/dP)_{II\to L}$, which may vary between 35 and 65

K GPa^{-1}.

Within this range, the minimum value that $1/X$ can assume is -0.0029 GPa K^{-1}. This is obtained for the extremal values

$$\Delta V_{L\rightarrow \mathrm{I}}=7\%,\quad (dT/dP)_{\mathrm{II}\rightarrow L}=65\ \mathrm{K\,GPa^{-1}}\ .$$

This means that the I→II phase boundary (Fig. 17) must lie *to the left* of the line with slope

$$\frac{dT}{dP}=-\frac{1}{0.0029}=-350\ \mathrm{K\ GPa^{-1}}$$

and have either larger negative values, or positive ones. This is dashed line E in Fig. 17 which crosses the 300-K isotherm at 14.6 GPa, taking the extremal coordinate for the triple point: $T_t=1050$ K, $P_t=12.5$ GPa. We do not give here, for brevity, the graph of the two-variable function of Eq. (7) which leads to this conclusion, but numerical verification is straightforward. For instance, a phase-boundary line that would go from the triple point to the previously accepted value for the transition (17 GPa at 300 K), has a slope of -170 K GPa^{-1}, that is $1/X=-0.006$, which is below the minimum of 0.0029 that we mentioned above. With this value, the closest one can come to the limits we set previously is $\Delta V_{\mathrm{II}\rightarrow L}=8\%$ and $(dT/dP)_{\mathrm{II}\rightarrow L}=70$ K GPa^{-1}, which is outside the values defined before. The reader may also easily verify that any other value of the parameters, e.g., for the triple point within the range that we discussed, will move the phase-boundary line to lower pressures at 300 K.

4. *Comparison with our results*

In Secs. III C 1–VII C 3 we showed that previously existing data alone did point to the accepted transition pressures at 300 K to be some 2 to 3 GPa too high. We can now incorporate our results into the picture. In Sec. V we reported observation of the transition at 13.6 GPa—or less—at 620 K. This is data point A in Fig. 17 which happens to fall on line E for no particular reason. Point B is from Ref. 16, where complete transition is observed by shock-wave methods at 16.2 GPa with an overheating of 70 °C which means T is in the vicinity of 360–370 K. Point C is the average value reported for observation of the transition by previous authors: 17.5 ± 1 GPa. The dotted line (D) which joins those three points must extrapolate to the triple point since it represents the classical decrease in temperature of the upstroke hysteresis. Its extrapolation above point A, although admittedly illegitimate, does nevertheless suggest that indeed 12.5 GPa is too high a pressure for P_t, as discussed above. Finally the results of Sec. VI, that is the I→II phase transition at 12 ± 1.5 GPa at 300 K, are shown as a heavy segment on the 300-K isotherm and the cross hatched region is the domain where the I→II phase-transition line is located. Actually as noted in Sec. III, the occurrence of planar defects which distort cubic GaAs at the onset of the transformation might well preclude any possibility of observing the actual equilibrium between the cubic and orthorhombic structures, and the martensitic character of this transformation may make the notion of "phase-boundary line" void of physical significance. What the crosshatched domain in Fig. 17 means is that at 300 K, cubic fourfold-coordinated GaAs is thermodynamically *unstable* above 13.5 GPa, and that orthorhombic, or in any case, sixfold-coordinated GaAs is unstable below 10.5 GPa. It does *not* mean that GaAs-II is the thermodynamically stable structure in an undistorted crystal at and above 13.5 GPa. It may well be that the occurrence of GaAs-II, which is close to the NaCl structure in any case, is induced by the anisotropic nature of the atomic collapse at the transition, and that it is not a stable structure at all, especially in view[10] of its small domain of existence (a few GPa), if it indeed does exist at all, as a bona fide structural variety.

VIII. CONCLUSIONS

In this paper a number of methods have been used to locate the transition between zinc-blende-structure cubic, and orthorhombic GaAs. Optical methods, x-ray diffraction, electron microscopy, Raman scattering, and x-ray absorption, *in situ* or at ambient, give different limits for the phase transition. Transport measurements were not discussed fully for brevity and because resistivity results are probably the most complex to analyze. One outstanding feature is that all those methods, taken individually, on the upstroke, alone, give conflicting results whereas, taken together, and on the upstroke and downstroke, they lead to converging conclusions (cf. Sec. VI). Another point to be noted is that, even if the direct and reverse transitions are completed and studied, each individual quantity taken as an *ad hoc* parameter for the hysteresis cycle gives the wrong result. There seems to be no alternative but to try to analyze the microscopic behavior of the lattice and relate it to the parameter under study.

This introduces the second point of this summary. The microscopic evolution of the atomic arrangement in the present case might seem complex at first sight: On increasing the pressure, the first step is towards sixfold coordination of local sites (13 GPa) and instability of twinning planes (15 GPa). This leads (16 GPa) to the onset of orthorhombic long-range order while a large fraction of the crystal is already sixfold coordinated. Microcrystals of the high-pressure phase take over at the expense of cubic GaAs which does not entirely disappear until ~22–24 GPa or so. On the downstroke, the same distinction occurs between the onset of local versus long-range ordering: the sixfold-coordinated fraction reverts to fourfold coordination by means of As-vacancy migration below 10 GPa. A large fraction of this transforms to the ordered zinc-blende structure between 7 and 0 GPa, whereas a smaller fraction of highly perturbed material can indeed anneal its interstitial-vacancy disorder and revert to fourfold coordination but not regain its crystalline periodicity and remains amorphous with fourfold coordination. At the phase transition from GaAs-I to GaAs-II, (i) the crystal symmetry decreases from zinc-blende-structure cubic to orthorhombic, (ii) the coordination changes from fourfold to sixfold, and (iii) nearest-neighbor distance increases. Those three quantities,

among others, are often taken to change simultaneously at the transition. Evidently they do not, and this makes the study of phase transitions at finite temperature somewhat arduous, which brings us to the next point: high-temperature measurements.

The point was made in the preceding section that in order to obtain the isotherm of any quantity in the P-V plane, especially on the highly desirable $T=0$ isotherm, *high*-temperature data were mandatory. Obviously, when studying highly reconstructive first-order transitions, the advantage of reducing the hysteresis is obvious, but this still does not give the full answer. Even with as careful an analysis as we tried to do here, to reduce the interval between the upstroke and the downstroke (Fig. 17) there still remains a domain of uncertainty where the extrapolation of the high-temperature phase-boundary line might not be as linear as we assumed, in the present—admittedly crude—estimate. The only alternative is then to construct the whole V-P-T diagram and to constrain it by thermodynamic arguments on the phase boundaries and on the isochores. This is not applicable only to GaAs. It is a general difficulty. This statement introduces another question: If indeed the I→II phase-transition pressure at 300 K has to be corrected from ~16 GPa down to some 12 GPa, why does this not apply to other crystals, notably the other III-VI compounds or group-IV elements? The answer is: It does.

The same variability in the estimates is found for this type of transition towards sixfold-coordinated structures, notably AlSb, GaP, InP, InAs, and GaSb and to a lesser extent Ge and Si. We have already obtained indications that the phase-transition pressure should be lowered in GaP, ZnSe, Si, and Ge, for instance. In Si,[40,41] resistance and photoconductivity measurements place the transition below 10 GPa. The same goes for Ge. In GaP, we had noted incipient opacity below 20 GPa in the course of our study of the phase transition[42] which we placed at 24 GPa at the time. In a recent paper[43] premonitory variations of the optical properties (band gap and absorption edge versus pressure) appear in GaP as low as 18 GPa, although the authors of the above reference did not analyze them. Indeed, by analogy with GaAs, where irreversible opacity as shown here occurs well above the pressure of instability for the zinc-blende structure, we can estimate the actual transition pressure for GaP to be below 18 GPa. Recently we found by Raman scattering that the onset of the transition in ZnSe (Ref. 44) was definitely below 12 GPa, this time in good accord with theory[19] and in contrast with the previously accepted value[45] of 14 GPa. Thus presently a revision of quite a few transition pressures might be in order especially above 10 GPa. This is all the more necessary as these systems, that is the column-IV elements and their binary isoelectronic analogues, have been chosen for calculations, notably for predictions of the stability of crystal structures and therefore serve as a test on the models and computational methods used. Indeed the goal of modern methods, *ab initio* or otherwise, is to predict all physical properties of solids under any structural modification, and, among others, the equation of state and the stability of one structure relative to the others in most cases on the $T=0$ isotherm. After the pioneer work of Phillips[4] and Van Vechten,[5–7] a number of other authors predicted with apparent accuracy the phase transitions and it could be claimed[19] that the greatest achievement of total-energy methods had been to predict the relative stability of semiconductor phases. So that up to 25 GPa, the "experimental" pressures versus calculated pressures fall close to a line of slope 1 with, nevertheless, notable exceptions. Actually for those semiconductors which have transitions above 10 GPa if one decreases the experimental pressures to the new values that we have found for Si, ZnSe, and GaAs, and that we have indications about, for GaP, one gets much lower correlation. As a concluding remark, nevertheless, one can note that a different estimate of the transition pressure and transition mechanism in GaAs had been published in one paper (Ref. 17) which showed that the total energy versus atomic displacement for a displacement pattern with orthorhombic symmetry close to the TA(X) mode had a second minimum and therefore instability for a pressure of ~8 GPa. This estimate is too low, probably because of an underestimate of the coefficient of the quadratic term in the expansion of total energy with atomic displacement. Nevertheless it is to be noted that this paper predicts the collective nature of the instabilities leading to the transition, the orthorhombic symmetry of the high-pressure phase, and a transition pressure as close to our estimate as other calculations, the latter two against "experimental" evidence since the high-pressure phase at the time was thought to be β-Sn or NaCl, and the transition pressure more in the 18-GPa range than in the range of 12 GPa.

ACKNOWLEDGMENTS

The GaAs samples used in this study were kindly provided by Dr. David Pitt, then at the Standard Telecommunications Laboratory in the United Kindom. One of us (J.G.) acknowledges support from the Consejo Nacional de Investigaciones Científicas y Tecnológicas (Venezuela) and the Centre National de la Recherche Scientifique (CNRS) (France). Physique des Milieux Condensés is Unité de Recherche Associée au CNRS No. 782.

[1] A. Jayaraman, R. C. Newton, and G. C. Kennedy, Nature (London) **191**, 1288 (1961).
[2] A. Jayaraman, W. Klement, Jr., and G. C. Kennedy, Phys. Rev. **130**, 540 (1963).
[3] A. Jayaraman, W. Klement, Jr., and G. C. Kennedy, Phys. Rev. **130**, 2277 (1963).
[4] J. C. Phillips, Phys. Rev. Lett. **20**, 550 (1968).
[5] J. A. Van Vechten, Phys. Rev. **182**, 891 (1969).
[6] J. A. Van Vechten, Phys. Rev. **187**, 1007 (1969).
[7] J. A. Van Vechten, Phys. Rev. B **7**, 1479 (1973).
[8] S. C. Yu, I. L. Spain, and E. F. Skelton, Solid State Commun. **25**, 49 (1978).
[9] M. Baublitz, Jr. and A. L. Ruoff, J. Appl. Phys. **53**, 6179 (1982).

[10]S. T. Weir, Y. K. Vohra, C. A. Vandenborgh, and A. L. Ruoff, Phys. Rev. B **39**, 1280 (1989).
[11]M. Hanfland, K. Syassen, and N. E. Christensen, J. Phys. (Paris) Colloq. **45**, C8-57 (1984).
[12]R. Trommer, E. Anastassakis, and M. Cardona, in *Light Scattering in Solids,* edited by M. Balkanski, R. C. C. Leite, and S. P. S. Porto (Flammarion, Paris, 1976), p. 396.
[13]B. Welber, M. Cardona, C. K. Kim, and S. Rodriguez, Phys. Rev. B **12**, 5729 (1975).
[14]J. Gonzalez, Thèse d'Etat, Université de Paris VI, 1988 (unpublished).
[15]A. R. Goñi, A. Cantarero, K. Syassen, and M. Cardona, High Pressure Res. **3**, 81 (1990).
[16]T. Goto, Y. Syono, J. Nakai, and Y. Nakagawa, Solid State Commun. **18**, 1607 (1976).
[17]K. Kunc and R. M. Martin, Phys. Rev. B **24**, 2311 (1981).
[18]S. Froyen and M. L. Cohen, Phys. Rev. B **28**, 3258 (1983); Solid State Commun. **43**, 447 (1982).
[19]J. R. Chelikowski, Phys. Rev. B **35**, 1174 (1987), and references cited therein.
[20]R. J. Elliott, Phys. Rev. **108**, 1384 (1957).
[21]R. Le Toullec, N. Piccioli, and J. C. Chervin, Phys. Rev. B **22**, 6162 (1980).
[22]W. P. Dumke, M. R. Lorenz, and G. D. Pettit, Phys. Rev. B **5**, 2978 (1972).
[23]Debye-Scherrer photographs from Ref. 14 are not shown here, for brevity. They are available from the authors on request.
[24]P. Gesecke and H. Pfistor, Acta Crystallogr. **11**, 369 (1958).
[25]M. L. Theye, J. Non-Cryst. Solids **77-78**, 1293 (1985).
[26]S. Amelinckx, R. Gevers, G. Remaut, and J. Van Landuyt, in *Materials Science* (North-Holland, Amsterdam, 1970).
[27]G. Thomas, R. H. Fulrath, and R. M. Fisher, *Electron Microscopy and Structure of Materials* (University of California Press, Berkeley, 1972).
[28]E. Dartyge, C. Depautex, J. M. Dubuisson, A. Fontaine, J. Jucha, and G. Tourillon, Nucl. Instrum. Methods A **246**, 452 (1986).
[29]H. Tolentino, E. Dartyge, and G. Tourillon, J. Appl. Cryst. **21**, 15 (1988).
[30]J. P. Itié, A. Polian, C. Jauberthie-Carillon, E. Dartyge, A. Fontaine, H. Tolentino, and G. Tourillon, Phys. Rev. B **40**, 9709 (1989).
[31]R. Le Toullec, J. P. Pinceaux, and P. Loubeyre, High Pressure Res. **1**, 77 (1988).
[32]P. Y. Yu and B. Welber, Solid State Commun. **25**, 209 (1978).
[33]R. K. Chang, J. M. Ralston, and D. E. Keating, in *Light Scattering Spectra of Solids,* edited by G. B. Wright (Springer-Verlag, Berlin, 1969), p. 369.
[34]J. M. Besson, G. Weill, J. L. Mansot, and J. Gonzalez, High Pressure Res. **4**, 312 (1990).
[35]M. Holtz, R. Zallen, O. Brafman, and S. Matteson, Phys. Rev. B **37**, 4609 (1988).
[36]R. S. Berg and P. Y. Yu, Phys. Rev. B **35**, 2205 (1987).
[37]G. Landa, Thèse d'Etat, Université Paul Sabatier, Toulouse, 1990 (unpublished).
[38]D. Strauch and B. Dorner, J. Phys. Condens. Matter **2**, 1457 (1990).
[39]M. D. Banus and M. C. Lavine, J. Appl. Phys. **40**, 409 (1969).
[40]E. H. Mokhtari, Thèse de Troisième Cycle, Université de Paris VI, 1988 (unpublished).
[41]J. M. Besson, E. H. Mokhtari, J. Gonzalez, and G. Weill, Phys. Rev. Lett. **59**, 173 (1987).
[42]J. P. Pinceaux, J. M. Besson, A. Rimsky, and G. Weill, *High Pressure Science and Technology,* Proceedings of the 8th AIRAPT Conference, Le Creusot, 1979, edited by B. Vodar and Ph. Marteau (Pergamon, Oxford, 1980), p. 241.
[43]C. Jauberthie-Carillon and C. Guillemin, J. Phys. Condens. Matter **1**, 6807 (1989).
[44]G. Weill (private communication).
[45]G. J. Piermarini and S. Block, Rev. Sci. Instrum. **46**, 973 (1975).

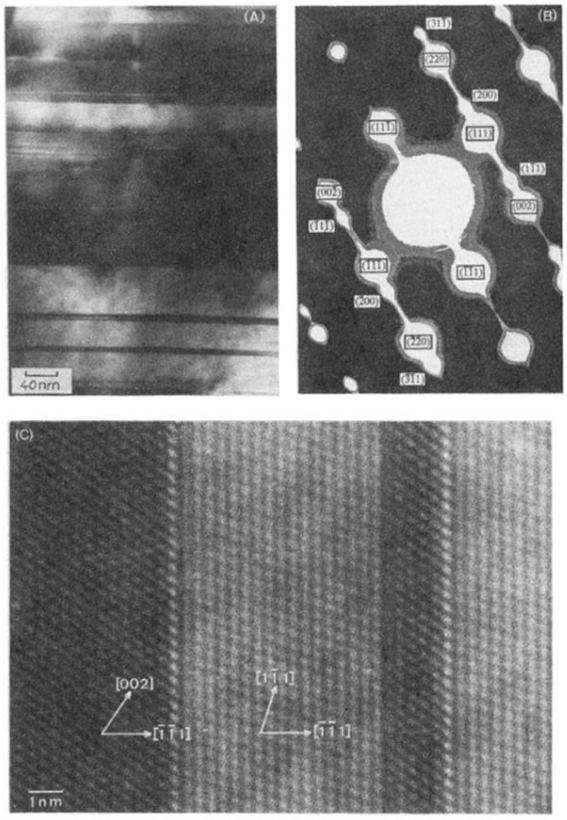

FIG. 7. Transmission electron microscopy of a sample taken to 17 GPa. (a) Low magnification micrograph showing twin planes between untransformed (dark) and transformed (light) regions. (b) Selected area electron diffraction on a zone 3 μm in diameter. Double spots are characteristic of twinned material. Common planes of the twinned crystals belong to the $[\bar{1}\,\bar{1}1]$ family. (c) High-resolution micrograph of transited (clear) and untransited (dark) regions. $(\bar{1}\,\bar{1}1)$ twin planes are normal to the plane of the figure and extend 5 to 8 nm in this direction, as calculated from the contrast.